LBL-19615
c.2

Lawrence Berkeley Laboratory
UNIVERSITY OF CALIFORNIA

Engineering Division

RECEIVED
LAWRENCE
BERKELEY LABORATORY
AUG 2 1985
LIBRARY AND
DOCUMENTS SECTION

ION IMPLANTATION OF BORON IN GERMANIUM

K.S. Jones
(M.S. Thesis)

May 1985

TWO-WEEK LOAN COPY
This is a Library Circulating Copy
which may be borrowed for two weeks.

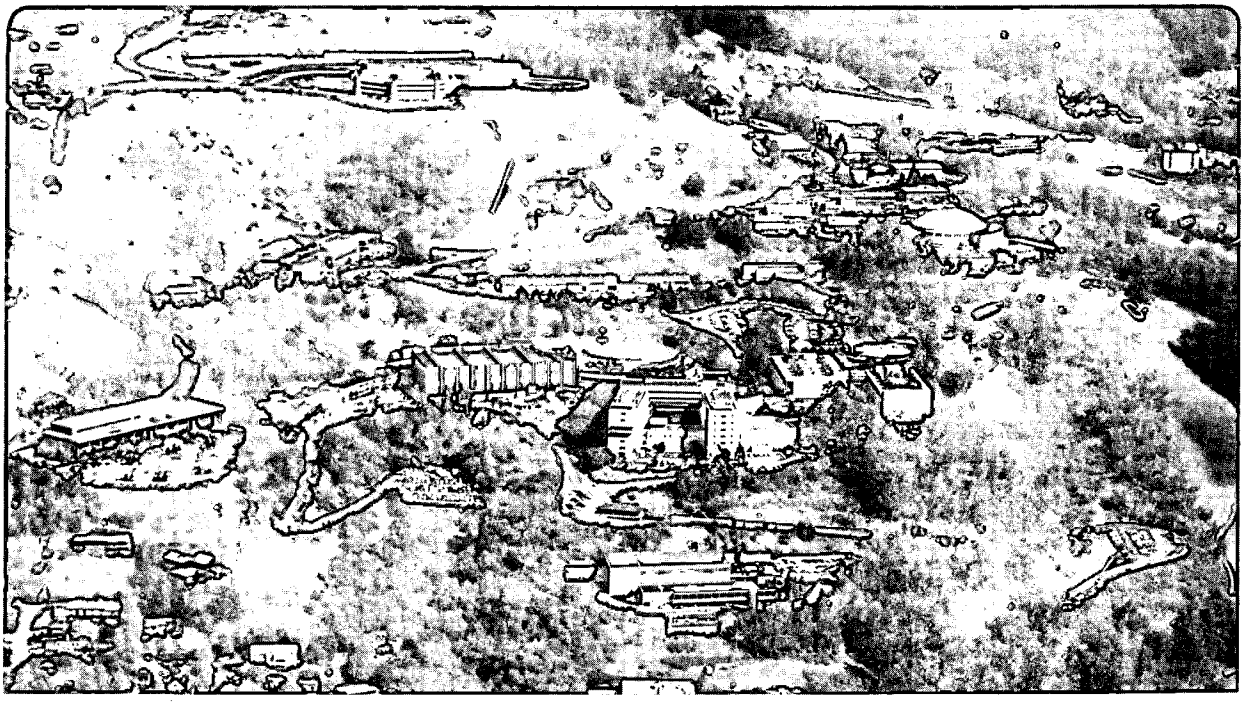

LBL-19615
c.2

Prepared for the U.S. Department of Energy under Contract DE-AC03-76SF00098

DISCLAIMER

This document was prepared as an account of work sponsored by the United States Government. While this document is believed to contain correct information, neither the United States Government nor any agency thereof, nor the Regents of the University of California, nor any of their employees, makes any warranty, express or implied, or assumes any legal responsibility for the accuracy, completeness, or usefulness of any information, apparatus, product, or process disclosed, or represents that its use would not infringe privately owned rights. Reference herein to any specific commercial product, process, or service by its trade name, trademark, manufacturer, or otherwise, does not necessarily constitute or imply its endorsement, recommendation, or favoring by the United States Government or any agency thereof, or the Regents of the University of California. The views and opinions of authors expressed herein do not necessarily state or reflect those of the United States Government or any agency thereof or the Regents of the University of California.

ION IMPLANTATION OF BORON IN GERMANIUM

Kevin Scott Jones

(M.S. Thesis)

Lawrence Berkeley Laboratory
University of California
Berkeley, California 94720

May 1985

ION IMPLANTATION OF BORON IN GERMANIUM

Kevin Scott Jones

ABSTRACT

Ion implantation of $^{11}B^+$ into room temperature Ge samples leads to a p-type layer prior to any post implant annealing steps. Variable temperature Hall effect measurements and deep level transient spectroscopy experiments indicate that room temperature implantation of $^{11}B^+$ into Ge results in 100 percent of the boron ions being electrically active as shallow acceptor centers, over the entire dose range ($5 \times 10^{11}/cm^2$ to $1 \times 10^{14}/cm^2$) and energy range (25 keV to 100 keV) investigated, without any post implant annealing. The concentration of damage related acceptor centers is only 10 percent of the boron related, shallow acceptor center concentration for low energy implants (25 keV), but becomes dominant at high energies (100 keV) and low doses ($< 1 \times 10^{12}/cm^2$). Three damage related hole traps are produced by ion implantation of $^{11}B^+$. Two of these hole traps have also been observed in γ-irradiated Ge and may be oxygen-vacancy related defects, while the third trap may be divacancy related. All three traps anneal out at low temperatures ($< 300°C$). Boron, from room temperature implantation of BF_2^+ into Ge, is <u>not</u> substitutionally active prior to a post implant annealing step of 250°C for 30 minutes. After annealing additional shallow acceptors are observed in BF_2^+ implanted samples which may be due to fluorine or flourine related complexes which are electrically active.

5/8/85

ACKNOWLEDGEMENTS

I am very grateful to Eugene Haller for the time and support he gave me during this project. I would also like to thank Stephen Pearton for his assistance and guidance during the initial stages of this study. I wish to extend my thanks to Nancy Haegel for the many fruitful discussions on Hall effect as well as all the encouragement. I am indebted to Robert McMurray for the help with the PTIS measurements and to Dick Chan for all of the implantations, often done without adequate notice. I also wish to thank Nathan Cheung for his discussions on BF_2. Finally, I am most grateful to Debra Dauphin-Jones for her patience and understanding.

This work was supported in part by the National Science Foundation, Grant DMR-8203430 and in part by the Director's Office of Energy Research, Office of Health and Environmental Research, U.S. Department of Energy under Contract No. DE-AC03-76SF00098.

TABLE OF CONTENTS

		Page
1.	Introduction.	1
	1.1 Review of Contacts on Semiconductors.	2
2.	Effects of Impurities and Point Defects	
	2.1 Electrostatic Properties	
	2.1.1 Free Carriers	9
	2.1.2 Ionized Impurities.	12
	2.2 Transport Properties	
	2.2.1 Mobility.	16
	2.2.2 Generation/Recombination.	18
3.	Ion Implantation.	20
	3.1 Theory	22
	3.2 Radiation Damage and Annealing	23
	3.3 Channeling	25
	3.4 Applications	26

4. Experimental Results. 28

4.1 Summary 28

4.2 Hall Effect 29

4.2.1 Implantation Species. 31

4.2.2 Implantation Dose Effects 32

4.2.3 Implantation Energy Effects 43

4.3 Deep Level Transient Spectroscopy 47

4.4 Other Experimental Results

4.4.1 Hall Mobility 56

4.4.2 Photothermal Ionization Spectroscopy . . . 60

4.3.2 Secondary Ion Mass Spectroscopy. 63

5. Summary and Conclusions. 66

References. 68

Appendix 1. 71

Appendix 2. 74

1. INTRODUCTION

Electrical contact formation is an integral part of semiconductor device fabrication. In the 1950's and 60's the most common electrical contacts were formed by either diffusing shallow level impurities into the semiconductor at high temperatures or applying a thin metal layer to the surface which formed a Schottky contact.

The potential application of ion implantation in the doping of semiconductors was realized around 1956[1]. By 1962 the first papers were published concerning the formation of thin contacts on nuclear radiation particle detectors.[2] During the late 1960's a large volume of work was being done with ion implantation, both commercially and in research applications. Today, as the size of devices in integrated circuits moves into the sub-micron range, ion implantation is becoming the most widespread method of selectively doping small areas of semiconductors.

Implantation of boron ions into germanium exhibits some unique phenomena. For every other ion implanted into silicon or germanium, some form of post implant annealing step is necessary to achieve a significant electrical activation of the doping species. However, implantation of boron at a typical dose of $1 \times 10^{14}/cm^2$ into germanium produces a peak acceptor center concentration of at least $1 \times 10^{18}/cm^3$ prior to annealing. This concentration is sufficient to achieve a p-type contact without a post implant annealing step. In fact, upon annealing the value of the sheet resistivity of a boron implanted layer shows no step decrease, characteristic of an implanted ion being activated.[3,4] Others have reported different results of a small resistivity step [5] and even a type change from n-type to p-type upon annealing.[6] One of the questions that arises is, what

is the source of the electrical activity associated with ion implantation of boron into germanium? Is the boron substitutional upon implantation and thus the source of the free holes or is the p-type conductivity due to lattice damage including possibly a variety of boron-defect complexes?

One reason for questioning the source of the conductivity, aside from its unusual annealing nature, is the published Rutherford backscattering (RBS) result[3] which shows a damage peak for 30 keV boron ions implanted into germanium. This damage peak is shown to anneal away by 170°C. Other observations include the effect of the temperature of the germanium during the implantation. As the substrate temperature drops from 130°C to -90°C the normalized disorder increases from 3 percent to 100 percent for a 56 keV, $6 \times 10^{14}/cm^2$ implant.[7] This result implies that a significant amount of annealing occurs around room temperature. Additional RBS results indicate that implantation of boron into germanium produces 10 times as much damage as implantation of boron in silicon for a dose of $1 \times 10^{15}/cm^2$ implanted at room temperature.[7] It is known that a post implant annealing step is required to electrically activate boron implanted into silicon. These two results might imply that the as implanted electrical activity of boron in germanium may be due to damage related acceptor centers.

From these results, it appears the nature of the electrical activity of implanted boron contacts on germanium is an issue worthy of further investigation.

1.1 Review of Contacts on Semiconductors

Doping group IV semiconductors with group IIIA and group VA elements is the most common method of altering the electrical proper-

ties of these semiconductors. When the majority of the free carriers originate from ionization of impurities the conduction mechanism is said to be "extrinsic". When a boron atom is in a substitutional semiconductor lattice site, it has only enough valence electrons to satisify three of the four covalent bonds which can be formed with its nearest neighbors. In order to complete its last bond, the boron impurity accepts an electron from the the host lattice thereby creating a positively charged hole in order to maintain the charge neutrality of the crystal. This hole is very weakly bound to the negatively charged boron impurity. The coulomb field of the negatively charged boron impurity is screened by the large static dielectric constant of the semiconductor (ε_r = 15.8 for Ge). In the hydrogenic model for an impurity in a semiconductor lattice both the static dielectric constant of the semiconductor and the effective mass of the carrier combine to reduce the binding energy of the carrier from 13.6 eV for the hydrogen atom to about 10 meV for a group IIIA or VA impurity in germanium. Due to this small ionization energy, for ultra-pure Ge at temperatures above 10 K, essentially all of these bound carriers are thermally ionized. The general effect of temperature on the free carrier concentration will be expanded on later. For germanium the Bohr radius of this weakly bound charge about the impurity site is approximately 80 Å. The large Bohr radius implies the spreading of the hole wavefunction over thousands of lattice unit cells. The resulting averaging is the reason why the effective mass theory leads to such accurate results in predicting the ionization energy of the impurity. If the concentration of impurities is high enough that the Bohr radii overlap, then conduction can occur without thermal ionization of the carriers. In germanium, this characteristic Mott

transition concentration can be easily calculated to be about 5 x $10^{17}/cm^3$. For tunneling ohmic contact purposes, it is necessary that this highly doped region be close to the surface.

Contacts are generally divided into two classes: ohmic and rectifying. Ohmic contacts are defined as those in which the contact offers negligible resistance to majority carrier flow to and from the bulk of the semiconductor. In order to make electrical contact to an outside circuit a metal-semiconductor interface must exist. The most common contact geometry is a metal-heavily-doped semiconductor-bulk semiconductor junction. Matching of the Fermi levels in the semiconductor and the metal result in band bending. Depending on the direction of the bending, a barrier against free carrier flow can exist. If the work function of the metal is such that a large barrier to current flow exists, then it is still possible to form an ohmic contact by making use of the phenomena known as tunneling[8] (see Fig. 1). Tunneling contacts are formed by heavily doping the semiconductor contact region near the metal-semiconductor interface, e.g. n^+ -n. At equilibrium the free carriers will exist in the lowest energy states. Due to this bending of the energy bands in real space, the interface will have a region void of free carriers. This depletion region with a characteristic width X_d, varies inversely with the square root of the doping density N_d.

$$X_d = \left[\frac{2\, \varepsilon_r \varepsilon_o\, \phi_i}{q\, N_d} \right]^{1/2}$$

where

$$\phi_i = \phi_m - X - \frac{(E_c - E_F)}{q} \qquad \text{(see Fig. 1)}$$

ϕ_m is the workfunction of the metal, X is the electron affinity of

the semiconductor and ϵ_r, ϵ_0 are the relative static dielectric constant and the permittivity of vacuum, respectively. In germanium doped with $1 \times 10^{19}/cm^3$ impurities and built-in potential ϕ_i of 0.2V, the characteristic barrier tunneling width is 59 angstroms. This width is small enough to allow significant tunneling. Under these circumstances the carriers necessary for conduction can tunnel through the barrier from the metal into the conduction band of the semiconductor and vice-versa, instead of having to acquire sufficient thermal energy to overcome the energy barrier, $q\,\phi_B$.

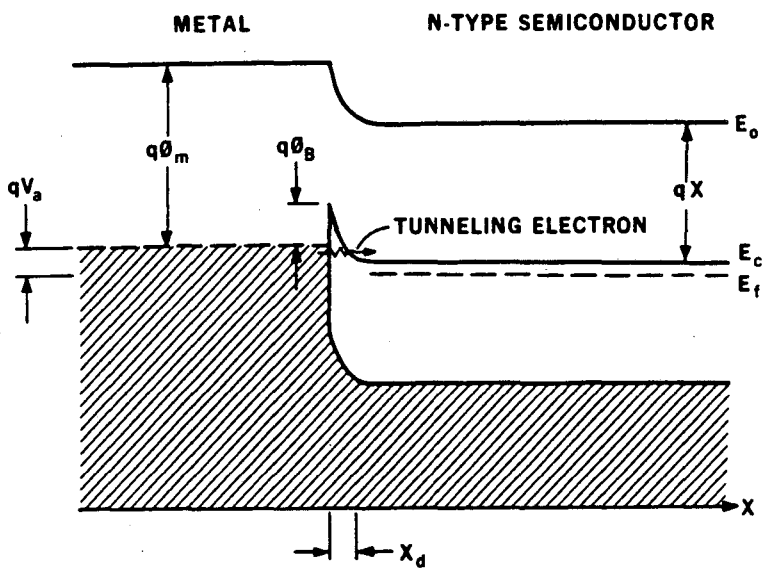

qØB: energy barrier to non-tunneling flow from the metal into the semiconductor

X: electron affinity

Øm: metal work function

XBL 853-1595

Fig. 1. Energy band diagram of a tunneling ohmic contact with an applied bias V_a.

A Schottky ohmic contact is formed when the majority carrier

concentration is higher in the contact region than in the bulk. This results when the metal-semiconductor interface band bending does not produce an energy barrier to majority carrier flow. This occurs between a n-type semiconductor and a metal with a work function smaller than the electron affinity of the semiconductor plus the energy difference between the Fermi level and the conduction band minima (see Fig. 2). An analogous situation exists for a p-type semiconductor and a metal with a work function larger than the electron affinity of the semiconductor plus the energy difference between the Fermi level and the conduction band minima. In both cases the result is the same, the majority charge whether negative or positive is accumulated at the surface of the semiconductor. This majority charge is then available for conduction into the semiconductor upon application of an electric field.

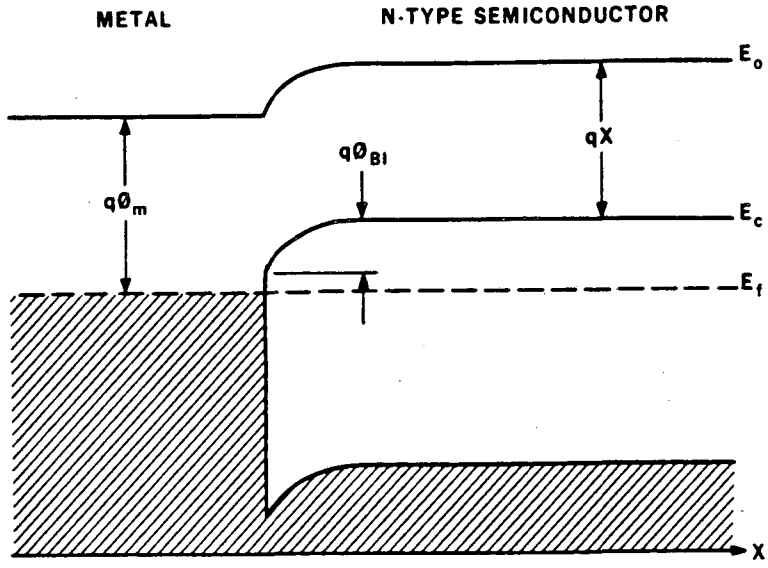

ϕ_{Bi}: built in or diffusion potential
X: electron affinity
ϕ_m: metal work function

XBL 853-1591

Fig. 2. Energy band diagram of a Schottky ohmic contact.

By definition, a rectifying contact is one in which carriers flow in one direction but not in the other. There are two common types of rectifying contacts: semiconductor junctions (p^+-n, n^+-p) and the Schottky barrier. The Schottky barrier involves making use of the energy barrier resulting from band bending at a metal-semiconductor interface. The work function requirements of the metal are just the opposite of what was discussed previously for the Schottky ohmic contact. For a Schottky barrier on a n-type semiconductor, the work function of the metal needs to be larger than the work function of the semiconductor which is defined as the electron affinity of the semiconductor plus the energy difference between the Fermi level and the bottom of the conduction band. In a p-type semiconductor, the work function of the metal needs to be smaller than the work function of the semiconductor for Schottky barrier formation.

This band bending model for metal-semiconductor contacts would be correct if not for additional complications such as surface states. Surface states at the metal-semiconductor junction can often dominate the electrical properties of the junction. They generally arise from lattice mismatch at the metal-semiconductor interface for metal-semiconductor junctions. They can also arise from impurities such as oxygen on a silicon surface and other effects due to the irregularity of the semiconductor surface. Surface states can "pin" the Fermi level of the semiconductor in the metal-semiconductor interface region and thus make the barrier height at the interface independent of the work function of the metal.[8]

Semiconductor junction contacts (p^+-n or n^+-p) involve doping the semiconductor with a large concentration ($>10^{19}/cm^3$) of an impurity that contributes carriers of type opposite to that of the

bulk. Internal band bending results upon equilibration of the Fermi levels. For either doped ohmic or p^+-n, n^+-p rectifying contacts, a large concentration of impurities is introduced in a relatively narrow region. This doping will result in a spatial concentration gradient of the free carriers which establishes a diffusion current as carriers move from a region of high concentration down this gradient. An electric field is created by the ionized impurities left behind upon diffusion of the free carriers. This electric field establishes a drift current which, in equilibrium, balances precisely the diffusion current.

P^+-n and n^+-p junctions have advantages as well as disadvantages when compared with Schottky barrier junctions. P^+-n and n^+-p junctions have lower reverse bias saturation currents when the doping of the bulk and contact are sufficient to produce a larger barrier height than the Schottky barrier height. It is also possible to inject minority carriers with semiconductor junctions which may be very useful. However, p-n junctions store charge when forward biased while Schottky contacts store less charge and thus can be switched into reverse status much more rapidly.

2. EFFECTS OF IMPURITIES AND POINT DEFECTS

2.1 Electrostatic Properties

To understand the methods used in characterizing ion-implanted layers, it is necessary to have a basic understanding of semiconductor physics. The electrical effects of impurities in semiconductors have two sources. The free carriers are responsible for electrical conduction while the ionized impurities represent a locally fixed space charge.

2.1.1 Free Carriers

The value of the Fermi-Dirac distribution function f(E) is the probability for occupation, by an electron, of an energy level at energy E:

$$f(E) = \left[\exp \frac{(E - E_f)}{k\,T} + 1 \right]^{-1}$$

where E_f is the Fermi energy. The density of states for the conduction band is given by:

$$N(E) = \frac{1}{4\,\pi^2} \left(\frac{2\,m^*}{h^2} \right)^{3/2} E^{1/2}$$

where m^* is the effective mass and h is Plancks' constant.

The integration of the product of the density of states in the conduction band and the Fermi-Dirac distribution function yields the number of electrons in the conduction band:

$$n = \int_{E_c}^{\infty} N(E)\, f(E)\, dE$$

Using the Boltzmann tail approximation, the number of free electrons n is given by:

$$n = N_c \exp \left[\frac{(E_f - E_c)}{k\,T} \right]$$

An analogous calculation yields the number of free holes p per unit volume which is given by:

$$p = N_v \exp \left[\frac{(E_v - E_f)}{k\,T} \right]$$

with the effective density of states for the conduction band N_c given by:

$$N_c = 2 \left(\frac{2 \pi m_e^* k T}{h^2} \right)^{3/2}$$

And the effective density of states for the valence band N_v is given by:

$$N_v = 2 \left(\frac{2 \pi m_h^* k T}{h^2} \right)^{3/2}$$

From these equations it can be seen that the temperature dependence of the free carrier concentration will be dominated by the exponential term with a slight effect arising from the $T^{3/2}$ dependence of the density of states. If the number of intrinsic free carriers (those excited from the valence band into the conduction band) substantially exceeds the doping concentration, then the Fermi level will lie near the center of the energy gap of the semiconductor and the number of free holes will equal the number of free electrons.

$$n = p = n_i$$

thus $$n\,p = (n_i)^2$$

or $$n_i^2 = N_c\, N_v \exp \left(\frac{-E_g}{k T} \right)$$

Therefore if the intrinsic concentration dominates, then a plot of the logarithm of the free carrier concentration versus 1/T should yield a straight line (ignoring the temperature dependence of the density of states) with a slope equal to the energy gap divided by 2k. Figure 3 is an idealized Arrhenius plot of the logarithm of the carrier concentration as a function of inverse absolute temperature.

The steep slope (1) corresponds to intrinsic carrier freeze-out discussed above. The adjacent region (2) is a plateau with a constant carrier concentration. This concentration corresponds to the net impurity concentration. Because shallow impurity levels are located very close to the corresponding bands, they become ionized at low temperatures and contribute to a constant free carrier concentration over a wide temperature range, i.e., the plateau. At sufficiently low temperatures the free carriers arising from the impurity levels will begin to "freeze-out" on the impurity sites since there will be insufficient thermal energy to excite them all. This "freeze-out" of the free carriers yields a slope (3) which is proportional to the energy level of the impurity. This last region actually has an additional slope change from being equal to 1/2 the energy level divided by k (the Boltzmann constant) to being equal to the energy

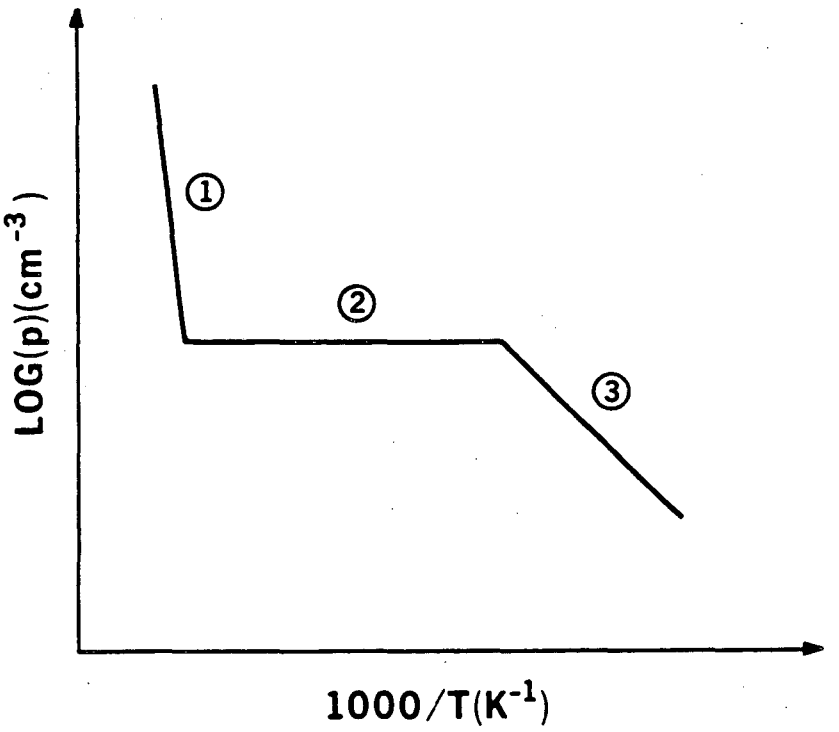

XBL 853-1593

Fig. 3. Arrhenius plot of the logarithm of the carrier concentration versus the inverse of the absolute temperature.

level divided by k. This slope change occurs when the free carrier concentration is equal to the concentration of compensating impurities, i.e., impurities of type opposite the dominant impurity. The reason for this slope change is due to the Fermi level shifting to the energy level of the dominant impurity in the band gap.

When investigating ion implanted layers, the concentration of the dominant impurity ($\sim 10^{18}/cm^3$ for $10^{13}/cm^2$ implant dose) is well above the concentration of the compensating impurities ($10^{12}/cm^3$). Thus any "freeze-out" slopes observed in this research correspond to an uncompensated "half slope" freeze-out.

2.1.2 Ionized Impurities

The ionized impurity concentration is the number of impurities that have given up a hole or an electron, respectively, to the lattice or to another impurity via compensation and now have a net charge. One method of studying ionized impurities involves a diode structure. The width of the space charge region, i.e., a region void of free carriers, can be used as a measure of the net impurity concentration. Many of the newer methods involve the study of current and charge transients produced by reverse bias pulses. In order to understand the effect of varying voltage on the depletion width, it is necessary to find a quantitative relationship between the various parameters. Poissons' equation relates space charge ρ to the electrical potential ϕ. The lateral dimensions of a p-n junction are typically much larger than the depletion width. Therefore we are concerned only with one dimension, and Poissons' equation reduces to

$$\frac{d^2\phi}{d\,X^2} = -\frac{\rho(X)}{\varepsilon_r \varepsilon_o}$$

where ε_r is the relative static dielectric constant for the semiconductor and ε_0 is the permittivity of vacuum.

In order to be able to integrate the above equation, it is necessary to know the doping distribution for the region around the junction. The space charge ρ is:

$$\rho = q\ (\ p - n + N_d - N_a\ )$$

where q is the charge of an electron, p,n are the free hole and electron concentrations and N_d, N_a are the ionized donor and acceptor concentrations, respectively. Assuming $\rho(X)$ is known, then single integration yields the electric field E as a function of X since

$$\frac{d\,\phi}{d\,X} = -\,E(X)$$

or

$$E(X) = \int \frac{\rho(X)}{\varepsilon_r \varepsilon_0}\ dX + C$$

The potential is usually composed of two parts, the built-in potential and the applied voltage. Before an external voltage is applied there naturally exists a "built-in" electric field which resulted from diffusion of free carriers across the junction and ionized impurities left behind as discussed previously. The region void of free carriers is known as the space charge region and integration of the "built-in" field over the entire space charge region yields the "built-in" potential. For germanium, a typical value for this "built-in" or "diffusion" potential ϕ_i is in the tenths of a volt range. Application of an external voltage can result in either an increase or decrease in the width of the space charge region depending on the polarity of the applied bias.

Double integration of the space charge density yields the potential as a function of X. For a given sum of the diffusion potential and the applied potential, the width of the space charge region X_d can be determined. For example, using the completed depleted approximation and the simple case of a junction with a X independent constant doping concentration on the p and the n side, respectively, the total depletion width X_d is:

$$X_d = \left[\frac{2\,\varepsilon_r \varepsilon_o\,(\phi_i - V_a)}{q} \left(\frac{1}{N_a} + \frac{1}{N_d} \right) \right]^{1/2}$$

where N_a is the acceptor concentration on the p-type side and N_d is the donor concentration on the n-type side. ϕ_i is the built-in potential and V_a is the applied bias.

In a p-n junction with constant doping on either side of the junction, the stored charge Q is:

$$Q = A\,q\,N_a\,X_p = A\,q\,N_d\,X_n$$

on the p-type and n-type sides of the junction, respectively. The area of the junction is A and $X_p + X_n = X_d$, the total space charge width. Because of charge neutrality $X_n = (N_a/N_d)\,X_p$. The differential capacitance C is:

$$C = \frac{dQ}{dV_a} = A\,q\,N_a \frac{dX_p}{dV_a}$$

from above

$$X_p = \frac{X_d}{1 + \frac{N_a}{N_d}}$$

$$\frac{dX_p}{dV_a} = \frac{1}{1 + \frac{N_a}{N_d}} \frac{dX_d}{dV_a}$$

Differentiating the above equation for X_d with respect to V_a and substituting back into the equation for the capacitance C yields:

$$C = \frac{\varepsilon_r \varepsilon_o A}{X_d}$$

This is the same as the capacitance of a parallel plate capacitor where A is the area of the plates, X_d is the distance between the plates and $\varepsilon_r \varepsilon_o$ is the dielectric constant of the material between the plates. Since X_d is a function of both the doping distribution and the applied voltage, if the applied voltage-capacity dependence is known, then the doping distribution can be calculated.

If one side of a junction is much more heavily doped than the other side, then the depletion width extends mainly into the lightly doped side. Under these circumstances, if the concentration distribution on the lightly doped side is constant, then the depletion width is given by:

$$X_d = \left[\frac{2\, \varepsilon_r \varepsilon_o\, (\phi_i + V_a)}{q\, N_a} \right]^{1/2}$$

or

$$C = \frac{\varepsilon_r \varepsilon_o A}{\left[\frac{2\, \varepsilon_r \varepsilon_o\, (\phi_i + V_a)}{q\, N_a} \right]^{1/2}} = A \left[\frac{q\, N_a\, \varepsilon_r\, \varepsilon_o}{2\, (\phi_i + V_a)} \right]^{1/2}$$

$$\frac{1}{C^2} = \frac{2\,(\phi_i + V_a)}{A^2 q\, N_a\, \varepsilon_r\, \varepsilon_o}$$

$$\frac{d(\frac{1}{C^2})}{d\,V_a} = \frac{2}{A^2 q\, N_a\, \varepsilon_r\, \varepsilon_o}$$

$$N_a = \frac{2}{q\, \varepsilon_r \varepsilon_o\, A^2\, (\frac{d\,1/C^2}{d\,V_a})}$$

The slope at each point in a $1/C^2$ vs V_a plot is inversly proportional to the doping density at the edge of the space charge region. This relationship is often used for profiling impurity concentration distributions. Schottky barrier contacts are often used for studying implanted regions as the profile is too shallow for a semiconductor contact, i.e., n^+-p, to be fabricated. As we shall see the lack of any Schottky barrier contacts to p-type germanium limits the applicability of this method for profiling boron implants.

2.2 Transport Properties

The discussion in this section will focus on those factors affecting the electrical transport properties which are directly related to experimental procedures used in this study. These factors are mobility and generation/recombination.

2.2.1 Mobility

The drift mobility μ is defined as the ratio of the drift velocity and a given electric field E:

$$\mu = \frac{v}{E}$$

When the kinetic energy of the carriers approaches or exceeds the thermal energy, the carriers become "hot" and the mobility becomes E field dependent. In the relaxation time approximation to the Boltzmann transport equation, t is the average time between collisions for a free carrier and the drift velocity is given by:

$$v = \frac{q\,t\,E}{m}$$

For holes:

$$\mu_h = \frac{q\,t}{m_h}$$

where m_h is the effective mass of the hole.

The resistivity ρ is given by:

$$\rho = \frac{1}{\sigma} = \frac{1}{n\,q\,\mu_e + p\,q\,\mu_h}$$

where σ is the conductivity and n, p are the electron, hole concentrations, respectively. Measurement of the resistivity of a sample will yield information only on the product of mobility and concentration. However, if both the resistivity and the carrier concentration are known as a function of temperature then the mobility as a function of temperature can be calculated.

Several factors can affect the time between collisions for free carriers and thus the mobility. The two major interactions are phonon scattering and ionized impurity scattering. At higher temperatures (300 K) most of the free carriers are scattered by lattice acoustical phonons. Since the concentration of these phonons exhibits a $T^{-3/2}$ dependence,[9] the mobility likewise shows a $T^{-3/2}$ dependence. Therefore, upon cooling in this temperature regime the mobility is

observed to increase. At lower temperatures (20 K) the number of phonons is small and the dominant scattering sites are the ionized impurities. This mechanism is known to have a $T^{3/2}$ temperature dependence[9] and thus the mobility decreases with decreasing temperature. Further elaboration on the subject can be found in Appendix 1.

2.2.2 Generation/Recombination

In addition to mobility effects, impurities can behave as generation/recombination centers or as trapping sites for free carriers. If a free carrier in either the conduction band or the valence band binds with an impurity site and then later is reemitted back to that same band then the impurity is called a trap. As there is a momentum difference between the minimum of the conduction band and the maximum of the valence band in an indirect band gap semiconductor such as Ge or Si, any recombination between carriers in these two bands must therefore involve a loss in momentum. This can occur with an electron, hole and phonon (three-particle process) or with the recombining charge making a transition to a delocalized energy level in k-space, losing its momentum difference at the intermediate energy level and continuing its decay (two-particle process). Deep level impurities are localized in real space and thus are delocalized in k-space. As a two-particle process is much more probable than a three-particle process, impurities that form deep levels dominate the generation/recombination processes in indirect gap semiconductors. The role of deep levels as recombination centers can be detrimental to devices requiring long carrier lifetimes and low reverse currents but are advantageous to fast switching devices.

The following derivation leads to the detailed balance relation which is the fundamental equation describing the emission rate of

carriers from impurity sites. Schockley and Read[10] and Hall[11] originally derived the equations to describe the generation/recombination processes. The SHR model is based on four possible processes. An electron can fall into a deep level or be emitted by a deep level and the same applies to a hole. The rates of these four possible transitions are defined as follows:

The rate of capture of a hole from the valence band is:

$$r_I = p < v_{th} > \sigma_p N_T F(E_T)$$

where $< v_{th} >$ is the thermal velocity, σ_p is the capture cross-section of the impurity for a hole and $N_T F(E_T)$ is the number of deep traps available to capture a hole. The emission rate for holes is:

$$r_{II} = e_p N_T (1 - F(E_T))$$

where e_p is the probability for emission of a hole and $N_T (1 - F(E_T))$ is the number of traps filled with a hole. Equivalent equations for electrons yield:

$$r_{III} = n < v_{th} > \sigma_n N_T (1 - F(E_T))$$

for electron capture and:

$$r_{IV} = e_n N_T F(E_T)$$

for the emission rate. The detailed balance relation can be derived

by noting that at thermal equilibrium:

$$r_I = r_{II} \quad \text{and} \quad r_{III} = r_{IV} \quad .$$

with

$$F(E_T) = \frac{1}{1 + \exp\left(\frac{E_T - E_f}{k\,T}\right)}$$

Thus for holes we find

$$e_p = \sigma_p < v_{th} > N_i \exp\left(\frac{E_i - E_T}{k\,T}\right)$$

where E_i is the intrinsic Fermi level energy. If the energy is referenced to the valence band, $\Delta E = E_T - E_V$, the emission rate becomes

$$e_p = \frac{\sigma_p < v_{th} > N_v}{g} \exp\left(-\frac{\Delta E}{k\,T}\right)$$

where g is the degeneracy of the trap usually assumed to equal 2 for germanium, N_v is the effective density of states in the valence band at T and ΔE is the energy difference between the trap level and the valence band. This value is only accurate if the temperature dependence of σ_p is known. The accuracy of the energy level determined is also limited by the degeneracy approximation. It will be shown later that this detailed balance relation is the basic equation used in experimentally determining several defect parameters by deep level transient spectroscopy.

3. ION IMPLANTATION

As stated in the introduction ion implantion of dopant species

has recently become a valuable technological tool. Due to the relatively small diffusion coefficients of most contact dopants, diffused contacts must be formed at high temperatures. The solution to this one dimensional diffusion problem with a solid-solubility limited surface concentration source of dopant is a complimentary error function, which describes the concentration of the dopant as a function of depth. Diffused contacts not only have large tail regions which extend into the crystal, they also have poor lateral resolution due to diffusion parallel to the surface. As device dimensions become sub-micron in size the lateral diffusion problem becomes more important. Ion-implanted contacts offer the ability to tailor concentration profile shape with sub-micron projected ranges. In addition, most of the implanted dopants can be "activated" at temperatures (~ 350°C for Ge) well below typical diffusion temperatures (> 600°C). For this reason, no high temperature processing is necessary, which reduces the likelihood of contamination via diffusion of unwanted species. Lower temperatures also mean less lateral diffusion so sub-micron doping becomes possible. It is also possible with ion implantation to achieve doping concentrations greater than the equilibrium solid solubility, although their electrical activity would be metastable at best.

Not all diffusion involves high temperatures. Lithium, an interstitial donor in germanium, is an example of a low temperature (<400°C) contact. The large diffusion coefficient of Li in Ge ($D_0 = 1.3 \times 10^{-3} cm^2/s$, $Q = 0.46eV$)[12] implies there will still be problems with lateral diffusion upon fabrication of the contact as well as further diffusion if any future annealing steps are performed on the device. Additional Li diffusion upon annealing was observed to be a

problem in DLTS samples prepared for this study. This will be further elaborated upon in the experimental section on DLTS studies.

No satisfactory p^+ diffused contacts can be produced at low temperatures (< 350°C) in Ge. As this is the temperature limit above which Cu contamination can become a problem, the need for ion implanted contacts is apparent.

3.1 Theory

Ion implantation involves the acceleration of ions in an electric field, separation of the various elemental species with a mass separator magnetic field, and finally, injection into a solid. For implanters using the pre-acceleration mass separation design, all of the implanted species are accelerated in the singly-ionized charge state, the notation "keV" will be used to describe the implantation energies. When an ion enters a crystal lattice, it can lose energy by two mechanisms. It can lose energy through elastic collisions between the ion and host lattice nuclei. The repulsive force F(r) in such collisions is coulombic of the form:

$$F(r) = \frac{Z_{1,eff} Z_{2,eff} e^2}{4\pi\varepsilon_0 r^2} \qquad \text{(CGS)}$$

Where Z_1e and Z_2e, the nuclear charge of the moving ion and the target atom, respectively, are reduced to $Z_{1,eff}e$ and $Z_{2,eff}e$ by the screening of the electrons. The distance between the incoming ion and the target atom is r and e is the electron charge. A hard sphere with a constant radius is often used to approximate this type of collision. The collision is termed elastic if after the collision the energy lost by the incoming particle is equal to the energy gained by the target atom. Elastic collisions account for most of the damage

done to the lattice as well as almost all of the angular deviations of the ion from its original trajectory. A sample damage calculation will be done later.

The second energy loss mechanism, termed inelastic scattering, arises from interaction of the accelerated ion with the electrons of the host lattice. This energy loss mechanism becomes more significant with decreasing ion mass and increasing implant energy, i.e., for boron implantation at energies above 11 keV.[1] The Lindhard, Scharff, Schiott[13] approximation to the amount of energy lost due to inelastic collisions $NS_e(E)$ is given by

$$NS_e(E) = 0.0793\, Z_1^{1/6} \frac{C_p}{C_\varepsilon^{1/2}} \left[\frac{Z_1 Z_2 (M_1 + M_2)}{(Z_1^{2/3} + Z_2^{2/3})\, M_1^3 M_2} \right]^{1/2} E^{1/2}$$

where Z_1, M_1 correspond to the atomic number and mass of the ion, and Z_2, M_2 correspond to the atomic number and mass of the target atoms. C_p is the Lindhard normalization constant for range (microns^{-1}) and C_ε is the Lindhard normalization constant for energy (keV^{-1}).

Combining the elastic and inelastic energy loss mechanisms, J. Lindhard and M. Scharff first proposed the statistical amorphous theory for ions in the keV energy range. This was later expanded and published by Lindhard, Scharff and Schiott, thus becoming known as the LSS theory. This theory has been used by Gibbons, et al.[14] to calcu- late the projected range and standard deviation for a number of ions implanted into various substrates.

3.2 Radiation Damage and Annealing

Although ion implantation has certain advantages over diffused contacts, i.e., highly doped submicron contacts which can be fabricated

at low temperatures, it has the disadvantage of causing radiation damage to the lattice during bombardment.

Below is a simple calculation of the number of Frenkel pairs (displaced atoms) produced per boron ion implanted into germanium. By the aforementioned equation for energy lost due to electronic processes, $NS_e(E)$, Gibbons, et al.[14] calaculates C_p to be 10.57 (microns^{-1}) and C_ε to be 0.04908 (keV^{-1}) for B in Ge. Using these values the electronic energy loss is 297 keV/μm while the nuclear energy loss is only 27 keV/μm for an implantation energy of 190 keV. Thus ~ 92 percent of the energy is lost by electronic interactions while the remaining 16 keV is lost via elastic collisions. The number of displacements can be approximated by:[15]

$$N(E) = \frac{6\,E}{\pi^2\,U}\ \ln\left(1 + \frac{U}{E_d}\right)$$

U is the energy to displace an atom from a substitutional site, E is the energy of the incoming particle lost via elastic collisions and E_d is the effective displacement threshold energy. Assuming $U = E_d = 4\,E_b$ where E_b is the bond energy, then:

$$N = \frac{0.42\,E_{elastic}}{E_{disp}}$$

The factor 0.42 arises primarily from the energy lost when an ejected atom has insufficient energy to create another Frenkel pair i.e. $E_d < E < 2E_d$.

The values which have been reported for E_d vary considerably at 300 K from 14.5 eV[16] to 22.3 eV[17,18]. The value of 22.3 eV was

used to calculate the minimum number of displacements using the equation above. For 190 keV $^{11}B^{+}$ implanted into Ge

$$N = \frac{0.42\ (15900)}{22.3} \sim 300 \text{ Frenkel pairs/ion}$$

For 25 keV ^{11}B in Ge N ~ 191 Frenkel pairs/ion. This may seem like a large number of displacements per ion. However, data for ion implantation of silicon into silicon[19] indicate that only 0.25 percent of all the Frenkel pairs created actually form electrically active defects that are stable at room temperature. The quoted experiment involved low dose implants ($1 \times 10^{10}/cm^2$) at 360 keV. Our carbon implantation experiments, presented in section 4.2.3, indicate as few as 0.05% of the defects created are both stable and electrically active at room temperature for 25 keV implants. Although most of the defects are annealed out at 300 K, it is still possible to have the damage contribute to or even dominate the total free carrier concentration via formation of levels in the bandgap.

3.3 Channeling

The channeling effect was discovered in the early 1960's. It was determined by computer simulation that heavy ions moving through a periodic array of atoms can be trapped in the interatomic channels which exist in certain low index crystallographic orientations. By avoiding elastic collisions, the ions can travel extended distances into the crystal leading to concentration profiles that are quite different from LSS predictions. The acceptance angle necessary for channeling can be approximated by:

$$\alpha_c = 0.3 \left[\frac{2 Z_1 Z_2 e^2}{4 \pi \varepsilon_r \varepsilon_o E d} \right]^{1/2}$$

where Z_1, Z_2 correspond to the ion, target atomic numbers respectively, E is the ion energy and d is the interatomic spacing of the target atoms in the direction of the channel. The table below gives the maximum calculated acceptance angle for a series of energies and orientations used during this study.

Energy (keV)	Ion	Substrate	Orientation	Angle α
25	^{11}B	Ge	<113>	2.4°
190	^{11}B	Ge	<113>	0.8°
25	^{11}B	Ge	<100>	2.6°
190	^{11}B	Ge	<100>	0.9°

By orienting the sample at least 8° off-axis, channeling effects were minimized during implantation. An additional form of channeling called random channeling can occur when an implanted ion is deflected via interaction with the host lattice into a major channel. A small percentage of ions are so deflected which leads to an extended "tail" region of the implant profile.

3.4 Applications

Aside from the unusual annealing characteristics, the study of ion implanted boron contacts in germanium is interesting from the viewpoint of its applications. One of the major uses of these contacts is as thin windows for nuclear radiation detectors. These detectors are made using ultra-high-purity germanium [$(N_d - N_a) \sim 1 \times 10^{10}/cm^3$]. The low impurity concentration of the material results

in a wide depletion region which performs as the sensitive volume of the detector. The detector is fabricated in the form of a diode and thus both high-quality p^+ and n^+ contacts are necessary. Another application of highly doped p-type contacts is for ohmic contacts used on infrared photodetectors[20] and low temperature bolometers[21].

For the case of nuclear radiation detectors there is a desire to avoid any high temperature annealing steps (> 350°C) which might result in contamination of the ultra-pure material by fast diffusing impurities. Copper is known to diffuse very rapidly in germanium with a diffusion coefficient as high as 10^{-5} cm^2/sec at 300°C. However the solubility is less than 10^{10} /cm^3 below 350°C. Copper is known to be a triple acceptor with three deep levels corresponding to $Cu^{---/--}$, $Cu^{--/-}$, $Cu^{-/o}$. In addition, copper forms electrically active complexes with hydrogen. As such, copper can be very detrimental to the energy resolution of radiation detectors since the various energy levels can act as trapping centers which can decrease the mean trapping length. For this reason it is desirable to avoid any annealing step which might result in copper contamination.

The group III-A elements are known from effective mass theory to produce shallow acceptors upon occupation of a substitutional site in group IV semiconductors. All of these five elements, thallium, indium gallium, aluminum and boron can form p^+ contacts upon implantation into germanium. As summarized by Ponpon, et al.[3] thallium and indium are the heaviest and thus produce the largest amount of damage during implantation. As such, they require a high temperature annealing step (> 350°C) in order to repair the lattice and electrically activate the species (i.e., move the implanted ion into a substitutional site).[22,23,24,25] Gallium has annealing requirements below 200°C

but only for low doses ($< 1 \times 10^{13}/cm^2$).[24] In order to operate at low temperatures (4 K) it is necessary to have a high dose so that impurity banding occurs and the implanted layer exhibits metallic conduction. Alton and Love[5] have shown the resistivity of aluminum implants in Ge to be twice that of boron implants for anneal cycles below 450°C and at a dose of $5 \times 10^{14}/cm^2$ (a typical dose for a heavily-doped contact). Therefore, boron which has annealing requirements below 350°C appears to be the best choice for a highly doped p^+ contact on germanium.

4. Experimental Results

Many experimental techniques were used to aid in understanding the unusual electrical nature of ion implanted boron in germanium. These included variable temperature Hall effect (VTHE), deep level transient spectroscopy (DLTS), photothermal ionization spectroscopy (PTIS), spreading resistance profiling and secondary ion mass spectroscopy (SIMS). Of these methods, VTHE and DLTS proved the most useful. For this reason the majority of the experimental evidence presented in this paper will be confined to these two methods and data from some of the other experimental techniques, including Hall mobility calculations, will be reviewed in the last chapter.

4.1 Summary

As there is a large quantity of data to be examined a brief summary of this data will be presented prior to the experimental evidence. In response to the questions posed in the introduction concerning the nature of the acceptor centers produced upon boron implantation, the results of the following experiments lead to several major conclusions.

The boron ions appear to be substitutional upon implantation over the entire dose range ($5 \times 10^{11}/cm^2$ to $1 \times 10^{14}/cm^2$) and energy range (25 keV to 100 keV) investigated. The proportion of damage related acceptor centers relative to the dose increases with increasing implant energy and decreasing dose. For doses below $5 \times 10^{12}/cm^2$, at high energy (100 keV), the damage related acceptor center concentration becomes greater than the substitutional boron related acceptor center concentration. These damage related acceptor centers anneal out at 250°C. The energy levels and annealing characteristics of the two major damage related acceptor centers correlate well with two hole traps previously observed in γ-irradiated germanium by Pearton *et al*[26]. They concluded the levels were associated with oxygen-vacancy related complexes.

Studies on unannealed 100 keV BF_2^+ implants indicate the boron is not significantly active prior to annealing and the damage related acceptor centers dominate at the two dose extremes studied ($5 \times 10^{11}/cm^2$, $1 \times 10^{14}/cm^2$). The damage shows the same annealing behavior as the boron implanted samples, although the BF_2^+ implants exhibit a greater amount of damage for the same energy and dose.

4.2 Hall Effect

Hall measurements are most commonly used to determine the free carrier concentration. The Van der Pauw[27] configuration, shown in figure 4, was chosen for our experiments. As the implanted layer is p-type from either damage related acceptor centers or substitutional implanted boron, a n-type ($2 \times 10^{11}/cm^3$) substrate was used in order to isolate the implanted layer upon cooling of the sample. The isolation process involves the formation of a p-n junction at the depth where the implant p-type concentration equals the substrates'

n-type doping. The electrical measurements are made via p-type (B) contacts which were implanted on the top surface corners and annealed prior to implanting the species to be studied. The germanium used is intrinsic at room temperature, therefore Hall effect measurements made at this temperature correspond to measuring the hole concentration in the implanted layer and the electron and hole concentrations in the intrinsic substrate. Upon cooling, the intrinsic carrier concentration decreases rapidly. Once the intrinsic carrier concentration is less than the n-type doping concentration of the substrate, electrons from the donor centers dominate the free carrier concentration of the substrate. At this temperature, a p-n junction forms in the tail region of the implanted layer and at subsequently lower temperatures, only the implanted layer is measured via the p-type contacts.

HALL EFFECT SAMPLE GEOMETRY

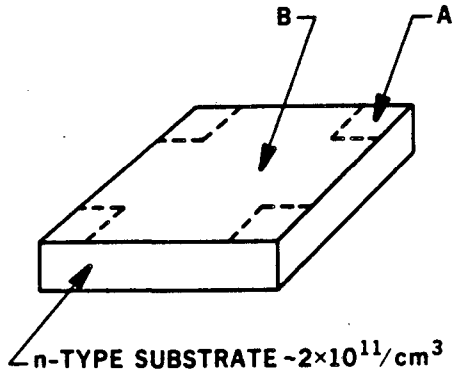

A: Ion implanted contacts on all four top surface corners (100keV B, $5\times10^{14}/cm^2$, annealed).

B: Ion implantation of the entire top surface with species to be studied.

XBL 8410-4377

Fig. 4. Van der Pauw Hall effect sample geometry for studying implanted layers

The Hall effect, using the Van der Pauw geometry, involves passing a current between two contacts on opposite corners and measuring the Hall voltage between the other two corners. This voltage arises from the Lorentz force exerted on the free carriers due to interaction with a magnetic field orthogonal to the implanted surface. The Hall coefficient is given by:

$$R_H = \frac{r}{p\ e} = \frac{t\ \Delta V_{13}}{B\ \ I_{24}}$$

where r is the Hall factor which is usually assumed to equal 1, B is the magnetic field, t is the thickness and ΔV_{13} is the Hall voltage between contacts 1 and 3 while a current I is passed between contacts 2 and 4. The thickness of the implanted layer is not accurately known; thus it is usually omitted and the carrier concentration is expressed as p•t in units of cm^{-2}.

There are three main parameters which can be changed in ion implantation. These are species, implantation dose, and implantation energy. All three of these parameters have been investigated using VTHE.

4.2.1 Implant Species

The species of most interest in this study is $^{11}B^+$. This ion was obtained using BF_3 as a source gas. In order to simulate the damage produced by $^{11}B^+$ implantation, $^{12}C^+$ was implanted and analyzed. Only singly ionized species were implanted and no other isotopes of boron or carbon were investigated thus all references to implantation of these elements will imply the ions $^{11}B^+$ or $^{12}C^+$ respectiveley. Substitutional carbon is isoelectronic with Ge and

thus upon implantation any free carriers must arise from damage related energy levels. The atomic weight and ionic radius of carbon is very similar to that of boron, making it an excellent species for the study of damage created by boron implantation. In addition to boron and carbon, BF_2 implants were, to a lesser extent, also investigated. There has been an increase of interest in the use of BF_2^+ instead of B^+ for the fabrication of implanted p-type contacts in Si. One of the primary reasons for this interest is due to the higher beam currents which are attainable with BF_2^+. As the most common source gas is BF_3, upon ionization the fraction of BF_2^+ ions is larger than that of B^+ ions. The increase in beam current due to the larger fraction of ions results in shorter implantation times for a given dose requirement and subsequently higher production throughput.

4.2.2 Implantation Dose Effects

In studying the effect of dose in these implantation experiments the energy of the implant was kept constant at 100keV. The dose range investigated ranged from $5 \times 10^{11}/cm^2$ to $1 \times 10^{14}/cm^2$. The latter dose is typical for a p^+ implanted contact. The projected range for a 100keV boron implant in Ge is around 2550 Å with a standard deviation of 1150 Å.[14] For a gaussian distribution the peak concentration, p, is:

$$p = \frac{\phi}{\sigma_p \sqrt{2\pi}}$$

where ϕ is the dose and σ_p is the standard deviation. For a $1 \times 10^{14}/cm^2$ implant dose the peak concentration is about $3.5 \times 10^{18}/cm^3$ which is well above the Mott transition concentration discussed in the introduction. Thus at this dose conduction, in the region whose

concentration is above the Mott transition, occurs via impurity banding due to the overlap of the electronic wavefunctions. The region of the implanted profile where the concentration is below the Mott transition affects the Hall coefficient and is responsible for the "dip" in concentration observed with VTHE of high dose (>1 x $10^{13}/cm^2$ for 100keV) implants. This will be expanded upon later.

By reducing the dose to 1 x $10^{13}/cm^2$ for a 100keV implant the peak concentration drops below the Mott transition and observation of a "freeze-out" slope of the thermally ionized free carriers becomes possible. At these low doses it is possible to use this slope to obtain information as to the binding energy of the centers creating the free carriers. Figure 5 shows VTHE plots for room temperature implants of boron at an energy of 100keV and a dose of 5 x $10^{11}/cm^2$.

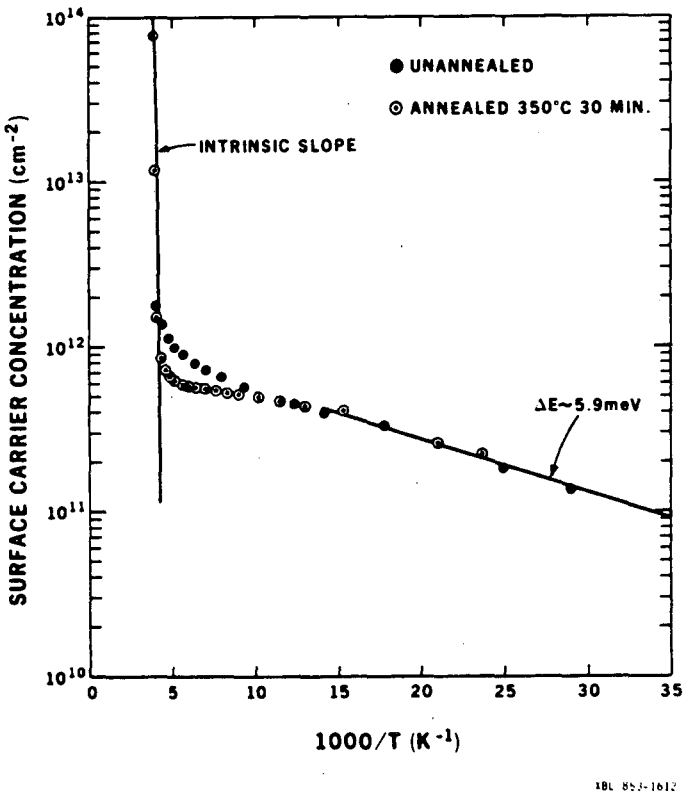

Fig. 5. Carrier freeze-out as a function of inverse temperature for a 100keV boron implant into Ge at a dose of 5 x $10^{11}/cm^2$.

Implants at this low dose were compensated for noise pick up by the Faraday cups in the implanter. At doses in this range ($<1 \times 10^{12}/cm^2$) as much as 10 percent of the signal recieved by the Faraday cups, which monitor the implant dose, can rise from noise. Compensating for this is necessary to implant the correct dose. All annealing steps in these studies were performed in a quartz tube furnace under an argon atmosphere for 30 minutes. The intrinsic freeze out slope in figure 5, is indicated by the dark line. The concentration of acceptor centers in the unannealed sample is about $1.5 \times 10^{12}/cm^2$ or about three acceptor centers per incoming ion which are stable at room temperature. After annealing at 350°C the concentration drops to around $8 \times 10^{11}/cm^2$. This decrease is due to the annealing out of damage induced acceptor centers. This will be further discussed later. The "freeze-out" slope for both samples is the same when the free carrier concentration drops below $5 \times 10^{11}/cm^2$ upon cooling. This slope corresponds to the "freeze-out" of an uncompensated energy level 10-12 meV above the valence band, which matches well with the predicted half-slope "freeze-out" of substitutional boron.

The VTHE plots for carbon and BF_2, also at an energy of 100keV and a dose of $5 \times 10^{11}/cm^2$, are shown in figure 6. The steep deep level slopes are similar to those observed in the unannealed boron curve in figure 5. This indicates that at an energy of 100keV and a dose of $5 \times 10^{11}/cm^2$, the acceptor center concentration in boron, carbon and BF_2 implants are all dominated by damage related centers. More damage is created by the BF_2 implant than the boron or the carbon implants. This is to be expected as the size and molecular weight of the BF_2^+ ion is much greater than the B^+ and C^+ ions. The effect of annealing the BF_2 implant is seen in figure 7.

The slope decreases as the deep damage related acceptor levels are annealed out and the boron is annealed into substitutional sites. If the boron were substitutional in the "as implanted" BF_2 implant as it is in the boron implant then the slope of the BF_2 implant (figure 7) should change abruptly to a shallow boron "freeze-out" slope as the

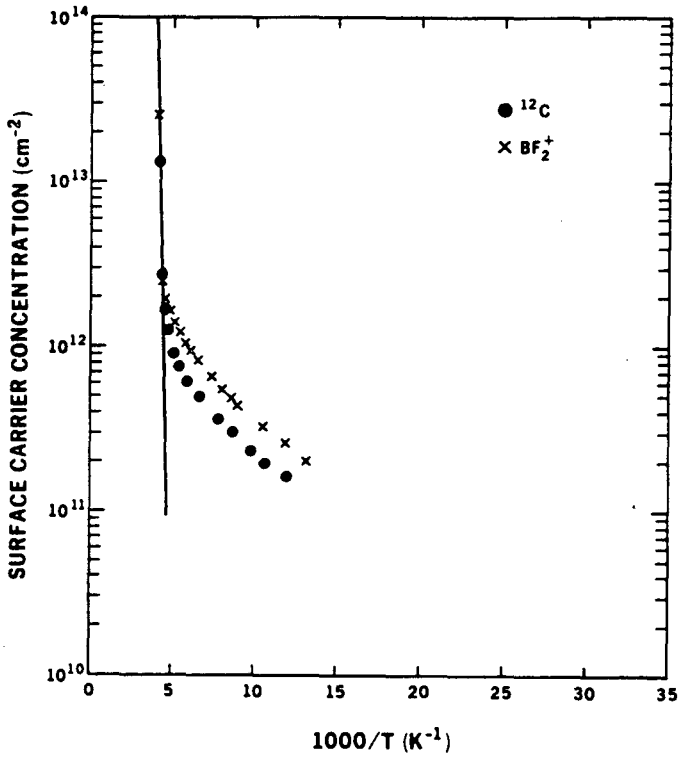

Fig. 6

Carrier freeze-out as a function of inverse temperature for unannealed 100keV implants at a dose of 5 x $10^{11}/cm^2$.

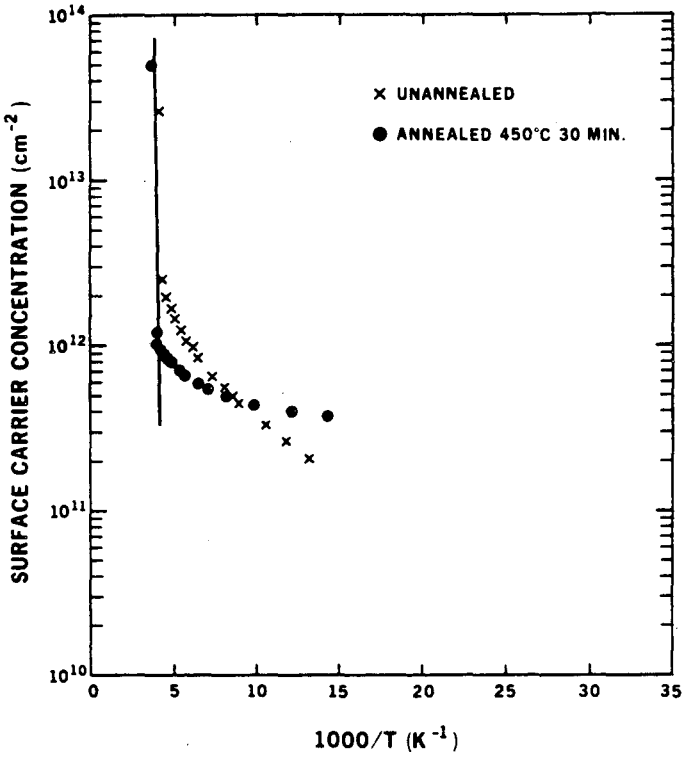

Fig. 7

Carrier freeze-out as a function of inverse temperature for 100keV BF_2 implants at a dose of 5 x $10^{11}/cm^2$.

free carrier concentration drops below 5 x $10^{11}/cm^2$. As the slope is still quite steep below 5 x $10^{11}/cm^2$, it is concluded that the boron in the BF_2 implant is not completely substitutional upon implantation and must be "activated" by an annealing step.

Figure 8 shows the effect of annealing on the total acceptor center concentration for all three implants at the implant energy of 100keV and dose of 5 x $10^{11}/cm^2$. The concentration was determined by the point at which the slope changed from an intrinsic freeze-out to a shallower slope. The difficulty in determining exactly where the slope changes from the intrinsic slope to the acceptor center "freeze-out" slope is expressed in the error bars shown. Implants of all three species exhibited an increase in the defect concentration upon annealing at 225°C. This may arise from the formation of additional defects due to increased diffusion of one of the species involved in the defect. This increase is also observed with DLTS. As will be seen, with our geometry, DLTS of these implanted layers does not yield an absolute concentration of the damage centers. Upon annealing there is observed a

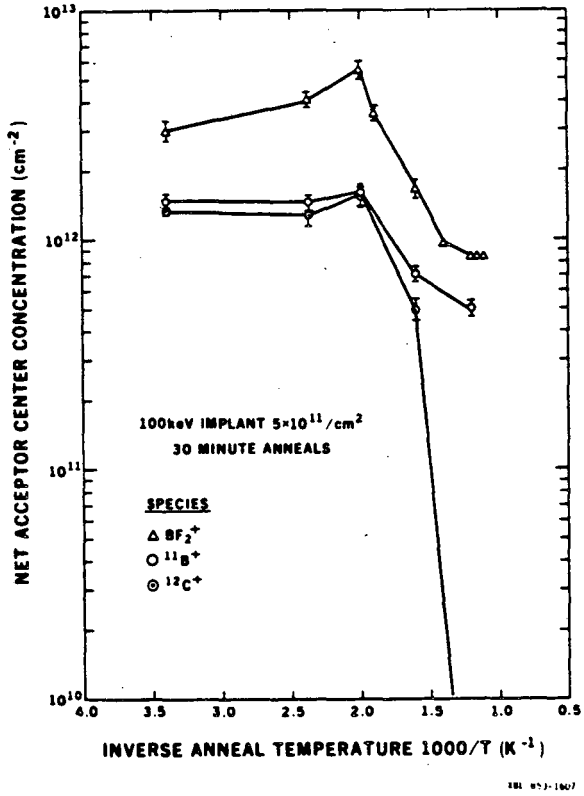

Fig. 8. Net acceptor center concentration as a function of inverse annealing temperature for 100keV implants at 5 x $10^{11}/cm^2$.

relative increase in the $\Delta C/C$ values (peak heights) which correlates well with the increase in acceptor center concentration observed with Hall effect. Annealing at temperatures above 250°C for 30 minutes dissociates the defect and above 350°C the carbon implanted samples return to being n-type, i.e., the p-type damage is annealed such that the background n-type doping is dominant. Subtraction of the carbon damage related acceptor center concentration from the boron related acceptor center concentration does not yield accurate quantitative information on the boron concentration as observed by the slope change in figure 5, noted previously. One explanation for this may be that carbon implants produce a slightly greater concentration of damage related acceptor centers, which are stable at room temperature, than the boron implants. Thus at this low dose, the carbon implants may have limited quantitative application to boron implants, but the qualitative annealing behavior for boron and BF_2 implants is sufficiently similar to the carbon implants behavior to conclude that damage related acceptor centers do indeed dominate this low dose, higher implant energy extreme. The concentration of acceptor centers in the boron implanted samples drops to about $5 \times 10^{11}/cm^2$ by 550°C while the concentration of acceptor centers in the BF_2 implanted samples drops only to $8 \times 10^{11}/cm^2$. The difference in concentration may be due to the fluorine being electrically active. This will be discussed later.

Contamination problems occured for anneal temperatures above 600°C. Additional investigations indicate that the n-type substrate changes to p-type at about 600°C due to Cu contamination. Precautions were taken to avoid contamination including a slow post-annealing cooling step to avoid "quenching in" large Cu concentrations by promot-

ing Cu precipitation.

The effect of increasing the dose on the acceptor center concentration in boron and carbon implanted samples is shown in figure 9. All samples were implanted at room temperature and were measured in the

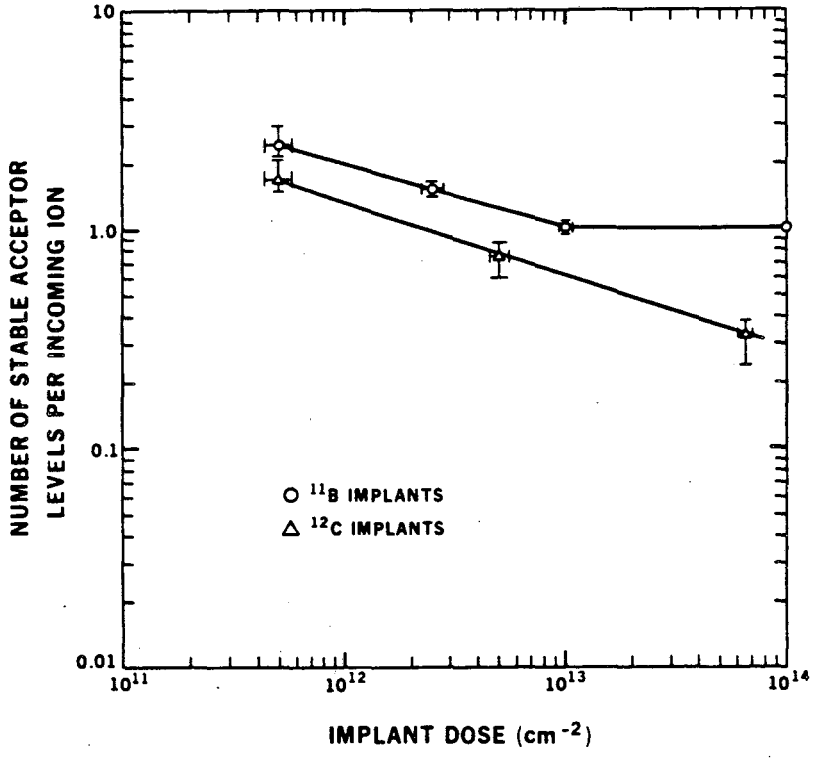

XBL 853-1605

Fig. 9. Net acceptor concentration as a function of implant dose for 100keV implants into Ge prior to annealing.

"as implanted" state. As the dose increases the number of defect-related, acceptor centers, stable at room temperature, per incoming ion decreases. However the concentration of acceptor centers arising from shallow acceptor levels becomes constant at one per incoming boron ion at doses above $1 \times 10^{13}/cm^2$. As we have just concluded that the boron is substitutional "as implanted" at the low dose extreme, figure 9 indicates that for a room-temperature 100keV implant the boron is active upon implantation over the entire range of doses studied. Any increase in free carriers at low doses must arise from

damage related acceptor levels and the concentration of these levels is greater than the concentration of shallow boron related acceptor levels at doses below $1 \times 10^{12}/cm^2$.

The VTHE results for a 100keV boron implant at a dose of $1 \times 10^{14}/cm^2$ are shown in figure 10. Implants of 100keV boron into Ge at doses greater than $1.5 \times 10^{13}/cm^2$ yield peak concentrations above the Mott transition and banding conduction occurs. For bulk Ge doped above $5 \times 10^{17}/cm^3$, the Hall coefficient, R_H, is independent of temperature.[28] However, as seen in figure 10, for implanted layers the Hall coefficient is not independent of temperature between 200K and 10K. This deviation can be explained theoretically by the following equation. Assuming there are no circulating currents and $\mu_H = \mu$ the surface Hall coefficient, R_s, can be expressed as[29]:

$$R_s = \frac{\int_0^t n(x)\ \mu^2(x)\ dx}{e\ [\int_0^t n(x)\ \mu(x)\ dx]^2}$$

where $n(x)$, $\mu(x)$ are the concentration and the mobility as a function of depth respectively. The junction depth is t.

Upon cooling through the upper temperature region (200K > T > 30K) the rapidly increasing mobility of the lower doped regions (those around the peak with concentrations less than $1 \times 10^{16}/cm^3$) contribute significantly to increasing the value of R_s. Upon further cooling the carriers in these lower doped regions (those not above the Mott transition) "freeze-out" and these high mobility regions become less of a factor in the value of R_s. The Hall coefficient upon cooling through this region (30K > T > 10K) decreases to a value

characteristic of just measuring the region of the implant above the Mott transition. The mobility of the highly doped region is relatively independent of temperature through this whole temperature range (200K > T > 10K). A rough estimate of the Hall coefficient, using the above equation, was calculated by dividing the implanted region into 17 sections of equal thickness and evaluating the integrals as sums of all the sections. For example, figure 12 is a combination of free carrier concentration and Hall mobility as a function of inverse temperature for a bulk germanium sample doped with $2 \times 10^{14}/cm^3$ gallium. In order to accurately determine the theoretical Hall coefficient curve, a plot such as this would be necessary for each section of the implant. The published values for the mobility as a function of temperature and concentration for p-type Ge just below the Mott transition are incomplete. As such, interpolation of mobility values was used and the low temperature values (T < 30K) became less accurate for concentrations between $5 \times 10^{15}/cm^3$ and $5 \times 10^{17}/cm^3$. The results of the calculations are shown in figure 13 along with the actual experimental data for both a bulk sample[28] and the implanted sample. The value of the bulk sample corresponds to the average concentration over the entire implanted layer. With no fitting parameters the initial high temperature theoretical values (T > 100K) are in good agreement with experimental values and the qualitative effect of temperature on the value of R_s is explained. The deviation in the quantitative theoretical values at lower temperatures may arise from inaccurate mobility and concentration values as a function of temperature in the concentration region discussed above or they may arise from deviation of the actual implant profile from its assumed gaussian shape due to perhaps random channeling.

Figure 11 shows that increasing the magnetic field decreases the magnitude of the increase in the Hall coefficient. This is due to magnetoresistance effects which decrease the mobility in the high

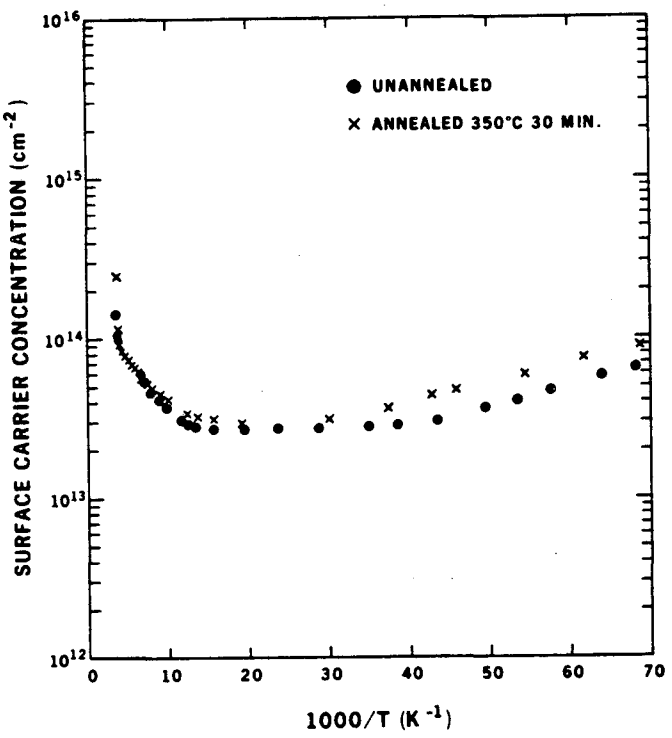

Fig. 10

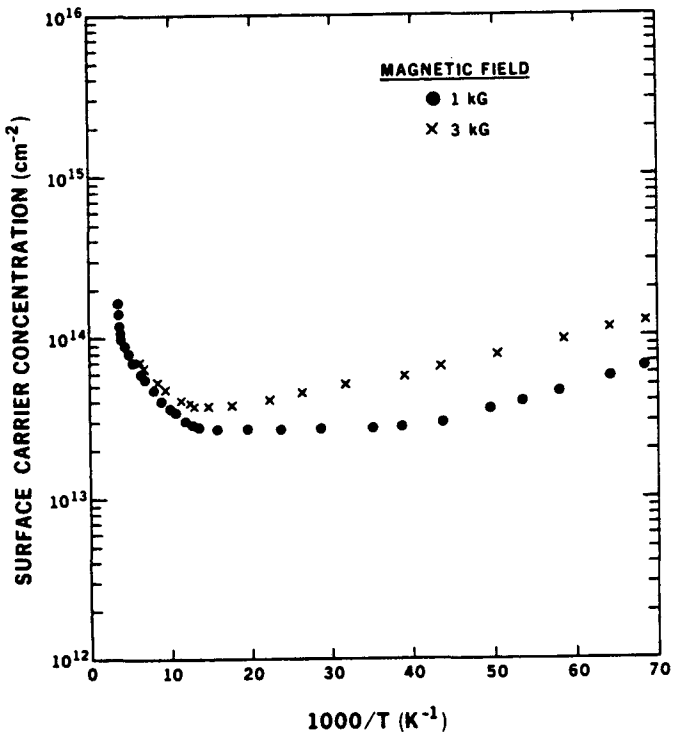

Fig. 11

Fig. 10-11. Carrier freeze-out as a function of inverse temperature for a 100keV boron implant of dose of $1 \times 10^{14}/cm^2$

mobility (lower doped) regions thereby reducing their influence on the Hall coefficient. Figure 10 indicates that there is little change upon annealing the boron implant. This is to be expected if, as we have concluded, the boron is active "as implanted".

BF_2 implants at 100keV and a dose of $1 \times 10^{14}/cm^2$, however, exhibit a very different behavior from boron implants as seen in figure 14. Prior to annealing some acceptor centers exist which may

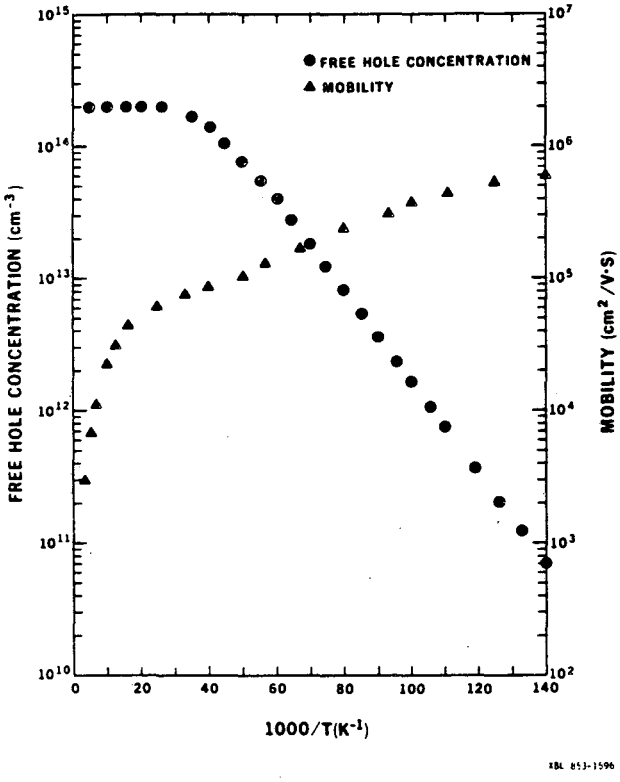

Fig. 12. Free carrier freeze-out and Hall mobility as a function of inverse temperature for a bulk Ga:Ge doped sample.

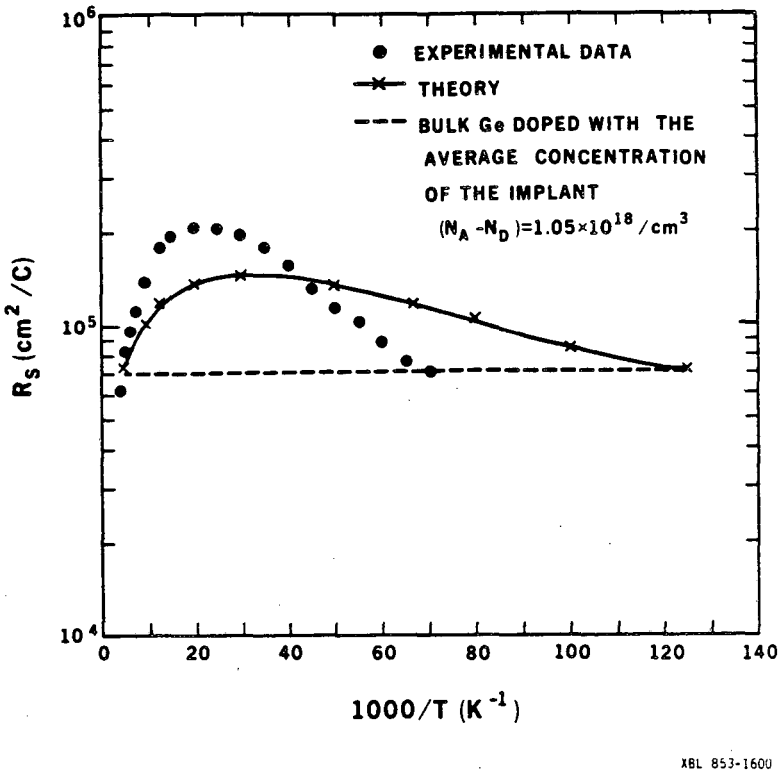

Fig. 13. The Hall coefficient as a function of inverse temperature for a 100keV boron implant in Ge of dose of $1 \times 10^{14}/cm^2$.

correspond to either damage related defects or some electrically active boron. The damage related levels will be discussed in the DLTS section. Upon annealing at 350°C for 30 minutes a significant change in the free carrier concentration is observed which corresponds to the boron becoming electrically active. In addition, as confirmed by DLTS, the damage is annealed out. The fact that there are more free carriers in the annealed state than implanted BF_2 ions could be explained in conjunction with some PTIS results to be presented. The additional holes may arise from interstitial fluorine atoms, which due

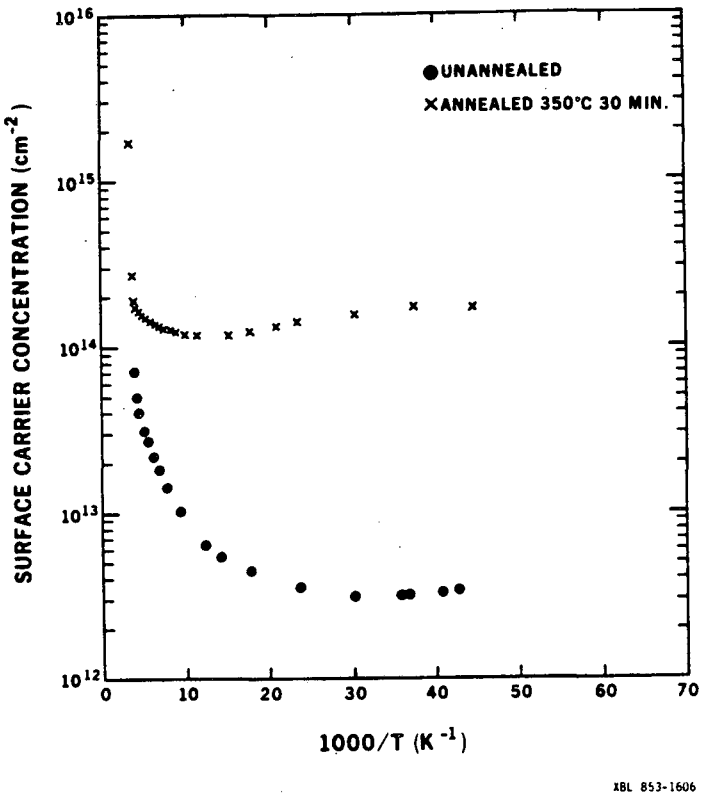

Fig. 14. Carrier freeze-out as a function of inverse temperature for 100keV BF_2 implanted into Ge at a dose of $1 \times 10^{14}/cm^2$

to their high electronegativity and relatively small size, could behave as interstitial acceptors in the same sense that lithium behaves as an interstitial donor in germanium. Initial VTHE results of $^{19}F^+$ implants indicate a shallow acceptor is formed whose concentration decreases (out-diffusion?) with increasing anneal temperature although it is still observed at temperatures above which all damage is repaired (400°C). As will be shown, a new set of acceptor lines are observed in PTIS experiments on annealed BF_2 implanted samples. Further investigation into this hypothesis is planned.

4.2.3 Implantation Energy Effects

What role does implant energy play in the question of the dominant

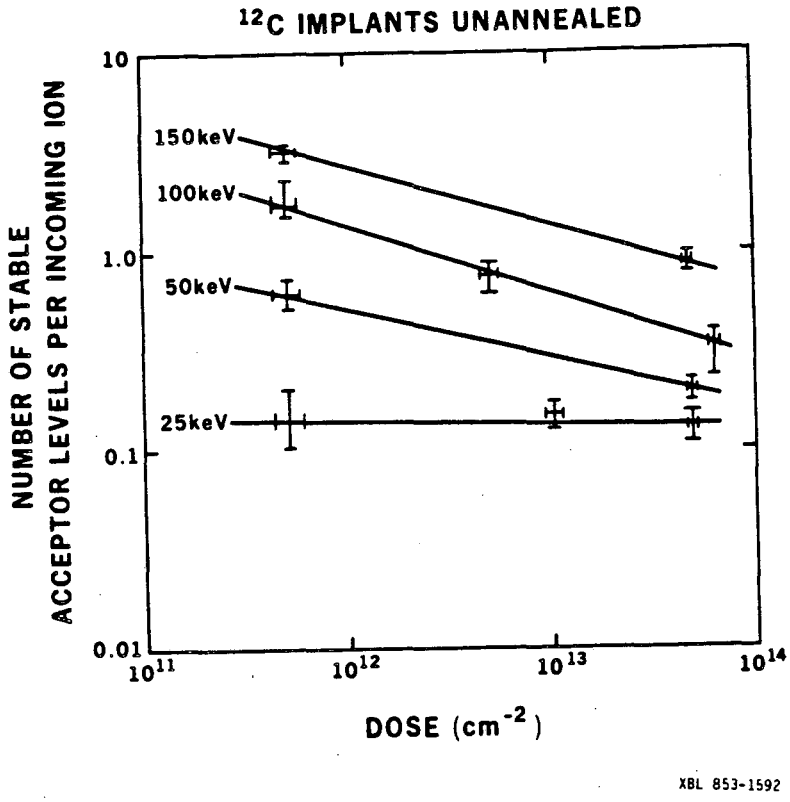

Fig. 15 Damage concentration as a function of implant dose for several implant energies.

energy level created by boron implantation? As was noted above, for 100keV implants the damage related acceptor level concentration does not exceed the substitutional boron acceptor concentration until the dose is below around 1 x 10^{12}/cm^2. Figure 15 shows the effect of changing the energy of carbon implants in the dose range of interest. As one increases the energy, the number of stable defects, for a given dose, increases. This trend is predicted by LSS[14] theory as there is more energy deposited elastically which creates defects. The number of stable defects observed is equal to the number created minus the number annealed or electrically inactive. LSS theory predicts a saturation of the number created at higher energies (>50keV) as a larger percentage of the energy is lost via inelastic scattering

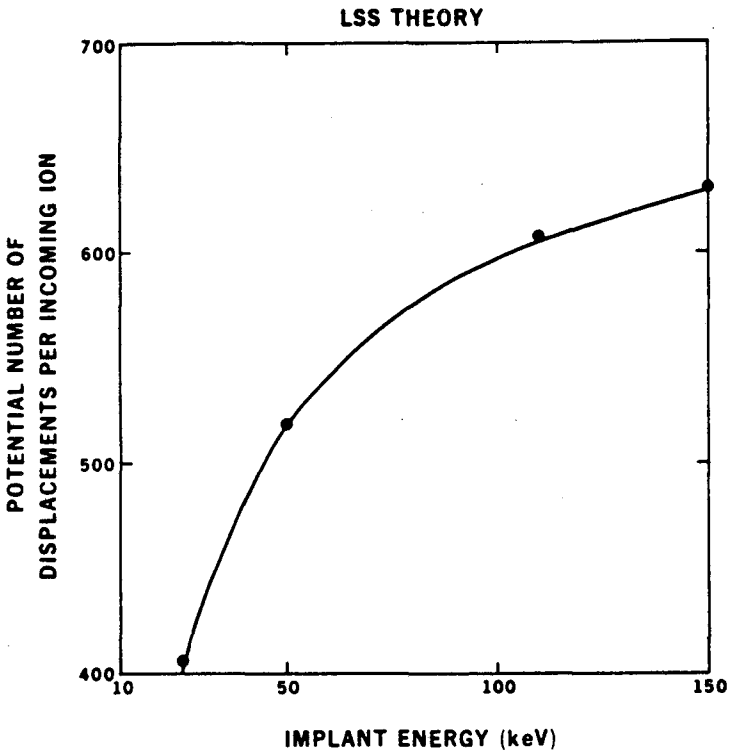

XBL 853-1598

Fig. 16

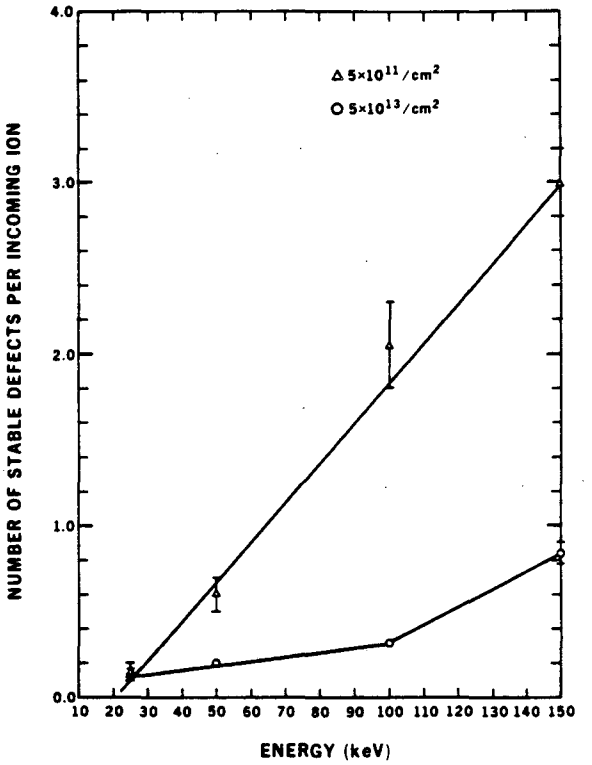

XBL 853-1597

Fig. 17

Fig. 16-17. Defect concentration as a function of implant energy.

(figure 16). As seen in figure 17, no such saturation was observed. However, as the number of defects created per incoming ion far exceeds the number observed, a direct correlation of the energy dependences of these two values should not be expected. As seen in figure 17 the number of stable defects per incoming ion increases much more rapidly at lower doses. Independent of the dose, at low energies (25keV) the number of defects per incoming ion is small. This is confirmed by figure 18. Again the boron is active "as implanted" and no significant change was observed upon annealing. From these results one could predict that a low dose ($5 \times 10^{11}/cm^2$) low energy (25 keV) implant should show only substitutional boron in the "as implanted"

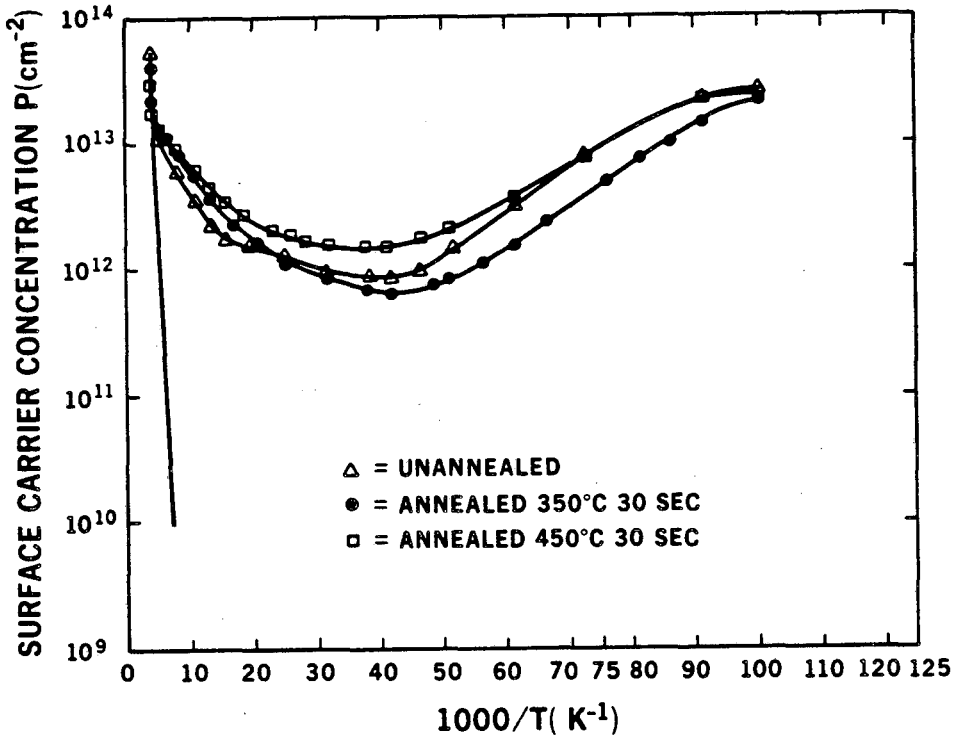

XBL 853-1594

Fig. 18. Carrier freeze-out as a function of inverse temperature for 25keV boron implants at a dose of 1 x 10^{13}/cm^2. The solid lines are not thoeretical fits.

state. This is observed in figure 19. The slope of the "freeze-out" line corresponds well to the expected uncompensated "freeze-out" slope of a shallow acceptor such as substitutional B in Ge. The reason no plateau is observed as in figure 5 is that the energy is less, therefore the peak concentration is greater for the same dose implant. It can thus be concluded that about 100% of the boron appears to be substitutional upon room temperature implantation at all doses and all energies studied. In addition, the relative concentration of damage related acceptor centers becomes significant at low doses and high

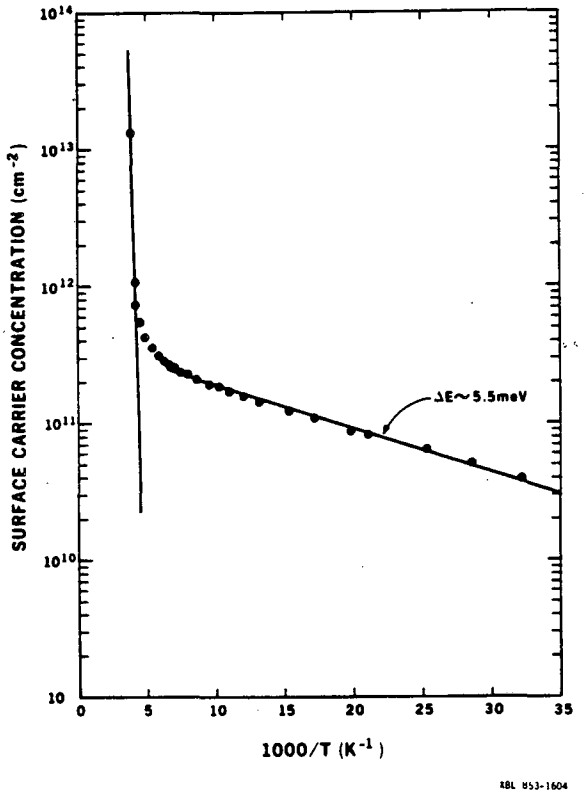

Fig. 19. Carrier freeze-out as a function of inverse temperature for a 25keV boron implant at a dose of $5 \times 10^{11}/cm^2$.

energies.

The next question concerns the nature of this electrically active damage created by boron implantation. The best experimental method to further investigate these deep acceptor levels proved to be deep level transient spectroscopy.

4.3 Deep Level Transient Spectroscopy

DLTS is the most common of the space charge capacitive transient spectroscopy techniques. Originally proposed by Lang[42], DLTS involves the application of a reverse bias to a p-n junction or a Schottky barrier diode, thereby creating a space charge region void of mobile carriers. The reverse bias is periodically reduced or pulsed back to

zero to allow the "filling" of ionized deep impurities. After the pulse, these trapped carriers are emitted from the deep level impurities. When deep levels trap charge carriers, they affect the depletion width upon reapplication of the reverse bias. This will change the capacitance of the junction. The reemission of bound carriers leads to a time dependent change in the capacitance of the reverse biased diode. The exponential time constant of the capacitive transient is a measure of the energy level of the trap.

Using the detailed balance relation derived on page 17 and the simple relationship $e_p = (t_p)^{-1}$, we find:

$$\ln t_p = \ln \frac{g}{\sigma_h \langle v_{th} \rangle N_v} + \frac{\Delta E}{k T}$$

where t_p is the emission time constant and all of the other variables are the same as identified on page 17. Experimental determination of t_p versus T was performed using a Miller correlator. An artificial exponential time constant is multiplied with the capacitive transient of the sample and the product integrated while the temperature is changed. When the capacitive transient of the sample equals the artificial transient a peak in the integrated product is observed. A plot of the natural logarithm of the emission time constant versus the inverse of the peak temperature yields essentially a straight line with a slope proportional to $\Delta E/k$, where ΔE is the apparent depth of the trap relative to the valence band for hole traps, as the temperature dependence of the capture cross-section could not be determined. The reason its not quite a straight line is that N_v and $\langle v_{th} \rangle$ are temperature dependent. Correction for the temperature dependencies of N_v and $\langle v_{th} \rangle$ is made by subtracting 2kT from the

above calculated value of ΔE.

The capture cross-section of a defect for the same carrier (electron for an electron trap) can be obtained from the y-intercept of this plot, as N_v and $\langle v_{th} \rangle$ may be calculated for a given temperature. The other technique commonly used to measure the capture cross-section involves observing the reduction in the number of traps filled as the pulse width is reduced. This technique measures the capture cross-section in the presence of an electric field, while the first technique yields the capture cross-section of a deep level in neutral material. The number of traps filled during a filling pulse, n(t), has an exponential dependence on the length of the pulse t and it is given by:

$$n(t) = N_T \left(1 - \exp(-t/\eta) \right)$$

where N_T is the total trap concentration and $\eta^{-1} = \sigma_h \langle v_{th} \rangle (N_A - N_D)$ is the inverse of the capture time constant of the trap. The capture cross-section for the hole trap is σ_h. N_T is usually determined from:

$$N_T = 2 \frac{\Delta C}{C} \left(N_D - N_A \right)$$

where ΔC is the capacitive transient for a saturating pulse. By using the relation derived previously for determining the net dopant concentration ($N_D - N_A$) from the capacitance-voltage relationship, and the relation above it is possible to determine the trap concentration (N_T) in the depleted region. If the pulse length is reduced from a saturating value to a shorter and shorter time eventually the DLTS

signal output will decrease. A plot of:

$$\ln \frac{N_T - n(t)}{N_T} \quad \text{vs.} \quad t$$

yields a straight line with a slope of η^{-1} and we find:

$$\sigma = \frac{\eta^{-1}}{\langle v_{th} \rangle \left(N_A - N_D \right)}$$

For the study of ion implanted layers with DLTS, several sample geometries were tried. As stated previously it is necessary to form either a p-n junction or a Schottky blocking contact to use DLTS. As no Schottky barriers to p-type Ge are known to exist, a p-n junction had to be fabricated. Attempts were made to fabricate a sample via implanting a low energy (25keV) phosphorus contact on one surface, activating the phosphorus by annealing and then implanting boron at a high energy (150keV) and low dose through the phosphorus contact. However this was not sucessful as the phosphorus contact was consistantly "deactivated" by the boron implant.

The geometry that eventually worked is shown in figure 20. It involves the fabrication of the p-n junction on the side opposite to that which has the implant to be studied. The sample was sliced thin enough (220μm) that under a reverse bias of 5 V, the main voltage drop occured in the implanted region. The p-type substrate doping was 2 x $10^{10}/cm^3$. It is desirable to know what reverse bias voltage is sufficient to deplete through the entire implant. In order to estimate this it is necessary to solve Poissons' equation for this geometry. One method of solving this problem is given in Appendix 2 and the

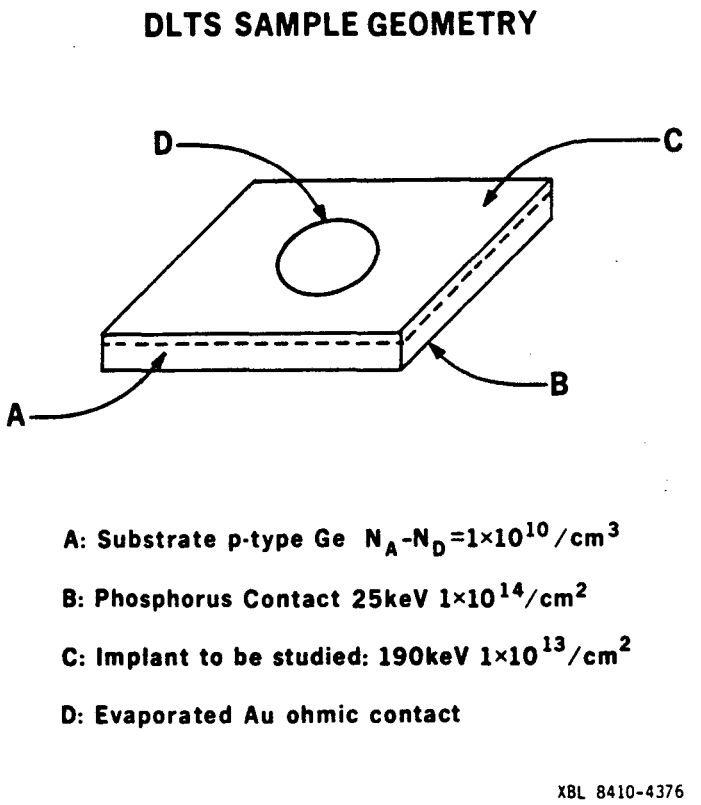

Fig. 20. DLTS sample geometry for study of implanted layers in Ge.

solution is shown in figure 21 (dashed line). As is seen in the figure, a reverse bias of 12 V would deplete almost entirely through a 190keV, 100% active, boron implant at a dose of 1 x 10^{13}/cm^2. A reverse bias of 8 V with a pulse of 7.4 V was used in the following experiments.

Figure 22 shows a comparison between 190keV implants of boron and carbon at a dose of 1 x 10^{13}/cm^2. The lowest spectrum shows a boron implant in the "as implanted" condition. The middle spectrum is of the same boron sample upon annealing at 140°C for 30 minutes, while the top spectrum is of a carbon implanted sample in the "as implanted" condition. All three spectra exhibit the same peaks except for the appearance of H4 in the carbon implanted sample. This implies that none of the damage peaks H1, H2 or H3 are boron related. It was not

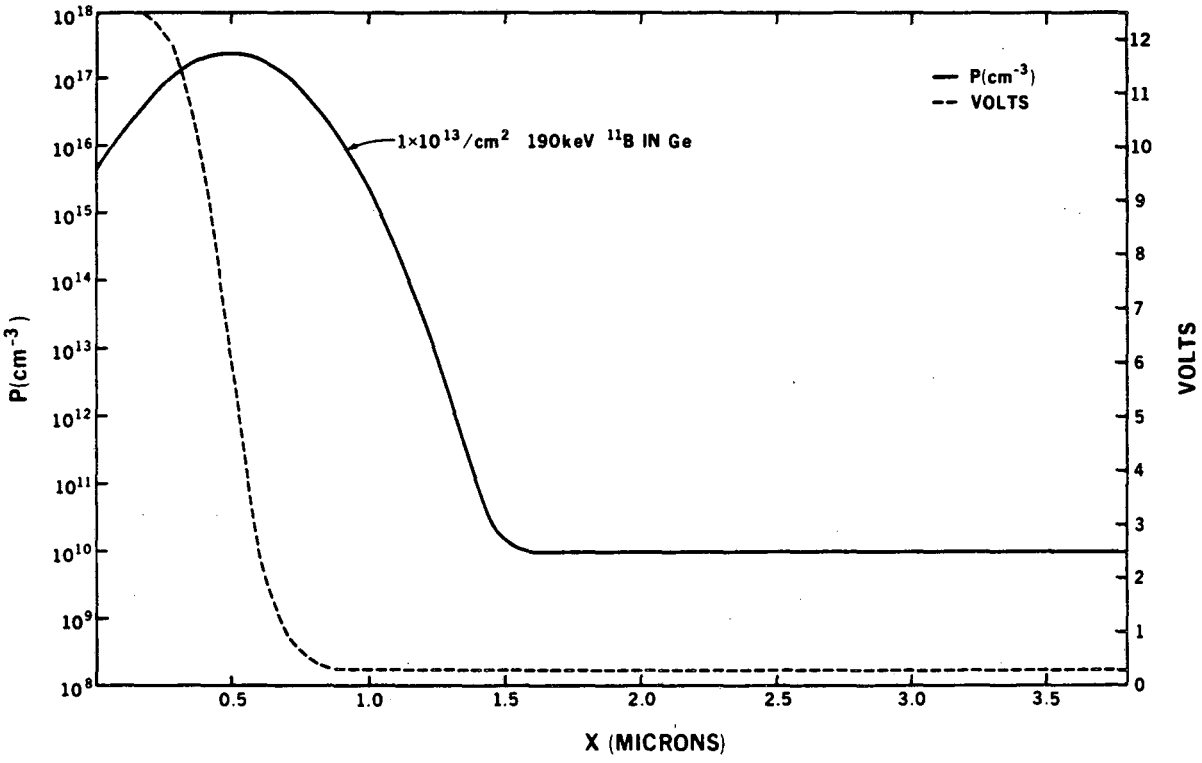

Fig. 21. Calculated voltage drop through a 190keV boron implant in Ge.

possible to determine the absolute concentration of these defects as the capacitance of the bulk dominates any C-V measurements and thus the background concentration is unknown. However, as will be shown, annealing studies imply that the peaks H1 and H2 are indeed the dominant damage related acceptor centers observed with VTHE. Figure 23 shows the characteristic correlator time constant, t, vs. 1000/T plot for H1, the hole trap at 110 K. The calculation of the energy level (E_v + 0.23eV) and the capture cross-section (2.24 x 10^{-12} cm^2) as determined from the y-intercept of the plot is also shown in this diagram. The table below lists the apparent energy levels and cross-sections for the various peaks. The hole traps H1, H2 and H3 also appear in samples implanted with BF_2^+, $^{14}N^+$, $^{16}O^+$ and $^{20}Ne^+$, which further indicates that they are independent of the

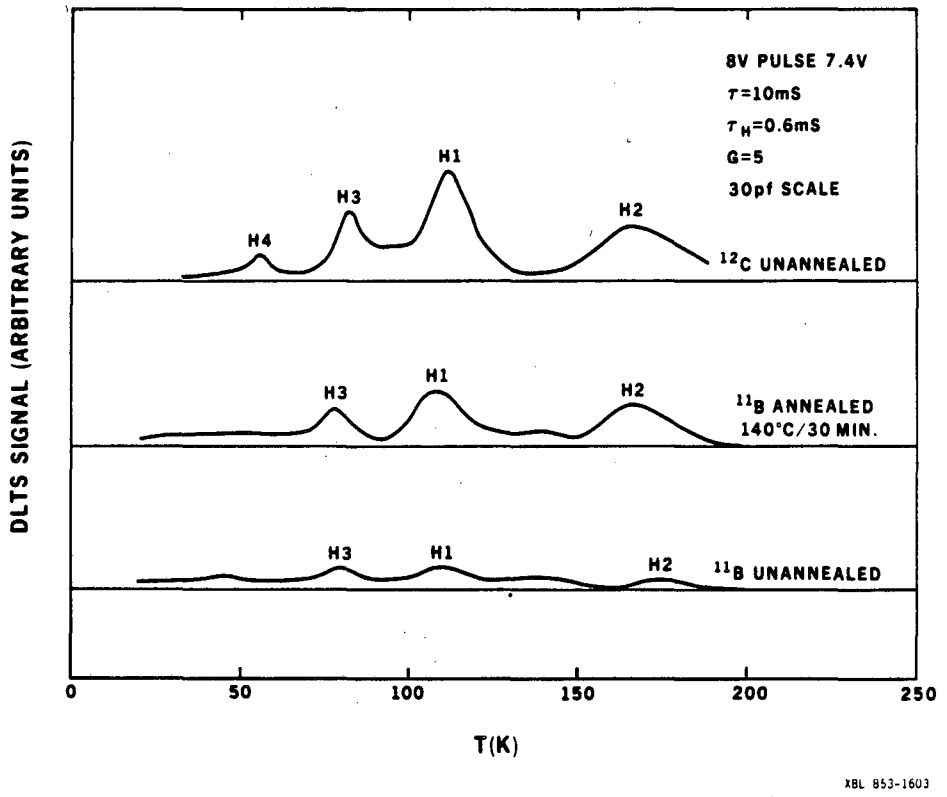

Fig. 22. DLTS spectra of 190keV boron and carbon implants in Ge.

species implanted.

Label	Temperature	Energy Level	Capture Cross-Section
H1	110 K	E_v + 0.23 eV	2.24×10^{-12} cm^2
H2	165 K	E_v + 0.37 eV	5.23×10^{-12} cm^2
H3	78 K	E_v + 0.17 eV	3.55×10^{-12} cm^2

From figure 22 it is seen that the trap peak heights increase when the sample is annealed at low temperatures (<250°C). This annealing behavior is summarized in figure 24 and results for the larger peaks H1 and H2 correlate well with the observed increase in concentration of the damage related acceptor levels in the low dose VTHE experiments discussed earlier (Fig. 8). In general, prior to annealing, the

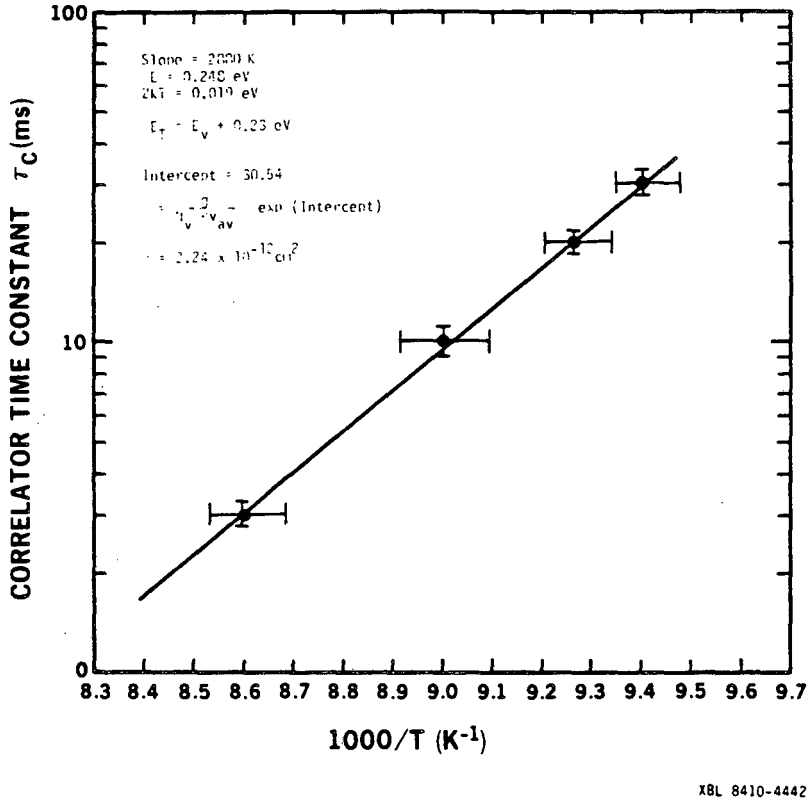

Fig. 23 Correlator time constant as a function of inverse peak height temperature for H1.

peaks for the boron implanted samples were smaller than the carbon implanted samples. This may be due to a slightly greater concentration of damage-related acceptor centers noted with low dose VTHE in figure 9, however it not does necessarily mean that the concentration of traps is greater, as the value of $\Delta C/C$ depends on both the number of traps and the average background doping in the region being observed with the pulse. Both of these are unknown, thus only relative changes in the ratio of these two unknowns can be observed with DLTS. VTHE experiments indicate the free carrier concentration in carbon implanted samples "freezes-out" rapidly upon cooling while the free carrier concentration in boron implanted samples remained high. If the trap concentration were the same in the two samples the value of

$\Delta C/C$, and thus the peak height, would be greater in the carbon implanted sample. If the shallow acceptor concentration is fairly constant upon annealing as the boron VTHE experiments indicate, then the change in $\Delta C/C$ plotted in figure 24 should correlate reasonably well with the relative change in the trap concentration upon annealing. By 250°C, both H1 and H2 have annealed away. This annealing behavior was observed regardless of the implant species.

The total capacitance of the sample (under a reverse bias > ~0.5V) is dominated by the capacitance of the bulk, not the implant region which is being filled and depleted of free carriers. The total capacitance change upon pulsing the voltage (i.e., 8V rev bias pulsing 7.5V forward bias) is very small and accordingly the value of ΔC relative to the C of the bulk is also very small. Thus a small $\Delta C/C$

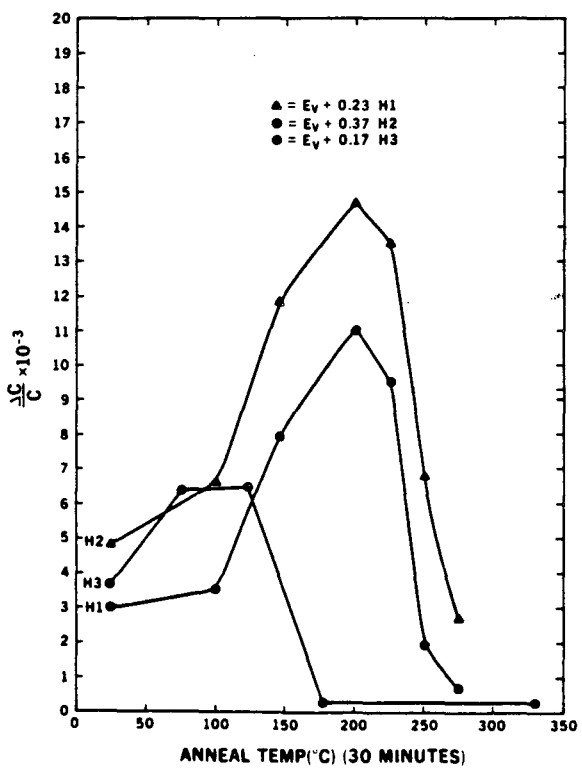

Fig. 24. Relative defect concentration as a function of anneal temperature.

does not necessarily mean a small trap concentration.

The energy levels and capture cross-sections of H1 and H2 match quite well with two hole traps observed by Pearton et al[26]. They found the same acceptor levels in γ-irradiated Ge and concluded they are oxygen-vacancy related complexes. To further substantiate the theory that H1 and H2 are the same peaks Pearton et. al. observed, the annealing characteristics of both sets of peaks are identical.

The hole trap H3 is observed to anneal out between 150-200°C. Bourgoin et al[30] have observed a hole trap with the same depth and similar annealing characteristics, using DLTS to study room temperature electron irradiated n-type germanium. They associate this hole trap and two electron traps with the divacancy.

The preliminary identification of all three hole traps H1, H2 and H3 is consistant with the observation of the traps being associated with damage induced, species independent levels. VTHE investigations using implantations of oxygen as well as other species are in progress to help determine if the major damage related acceptor centers involve oxygen. Sources of oxygen such as "knock-on" oxygen from the surface and oxygen grown into the crystal must be recognized in interpreting the results.

Upon annealing at higher temperatures (>300°C), Cu peaks were observed to grow confirming our suspicion that Cu contamination was the reason for the substrate conversion observed upon high temperature annealing of VTHE samples.

4.4 Additional Experimental Results

4.4.1 Hall Mobility

From the introduction it can be seen, that by measuring the free

carrier concentration and the resistivity as functions of temperature the mobility can be determined. Figure 25 shows the Hall mobility calculated from resistivity data and Hall effect data presented in figure 5 for unannealed 100 keV boron implanted at a dose of 5 x $10^{11}/cm^2$. The three regions of the mobility curve, discussed in Appendix 1, are evident. At 250 K, after the isolation process is complete the Hall mobility is about 1000 $cm^2/V\bullet s$. Assuming a $T^{-3/2}$ temperature dependence the mobility extrapolates back to about 750 $cm^2/V\bullet s$ at room temperature. For bulk Ge a room temperature drift mobility of 750 $cm^2/V\bullet s$ is observed in p-type samples doped at 1.5 x

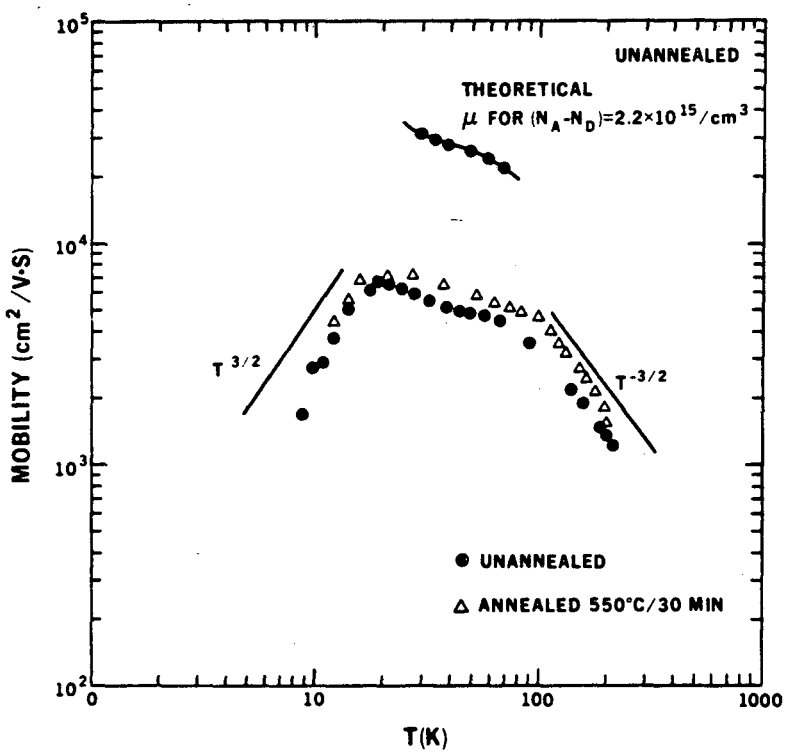

XBL 853-1601

Fig. 25. Hall mobility as a function of temperature for a 100keV boron implant into Ge at a dose of 5 x $10^{11}/cm^2$.

$10^{17}/cm^3$.[31] From Hall effect (Fig. 5) we observed a deep acceptor concentration of about 1.5 x $10^{12}/cm^2$. For a 100keV gaussian implant the peak concentration would be about 5 x $10^{16}/cm^3$. Thus

the mobility indicates a highly doped region ($>10^{16}/cm^3$) is being measured.

At high temperatures the acoustic phonons dominate the temperature dependence of the mobility. Upon cooling below 100 K there is a transition region where the dominant scattering mechanism switches from acoustic phonon scattering to ionized impurity scattering. The theoretical mobility values for $N_a-N_d = 2.2 \times 10^{15}/cm^3$ are also shown.[32] Below 20 K ionized impurity scattering dominates. The mobility in this region matches the theoretical mobility for $N_a-N_d = 8 \times 10^{16}/cm^3$ and the high field data (6 kG) for N_a-N_d = 2-3 x $10^{16}/cm^3$.[32] Again this correlates well with the peak concentration of the implanted layer. Also shown in the same figure (25) is the result after annealing the sample at 550°C for 30 minutes.

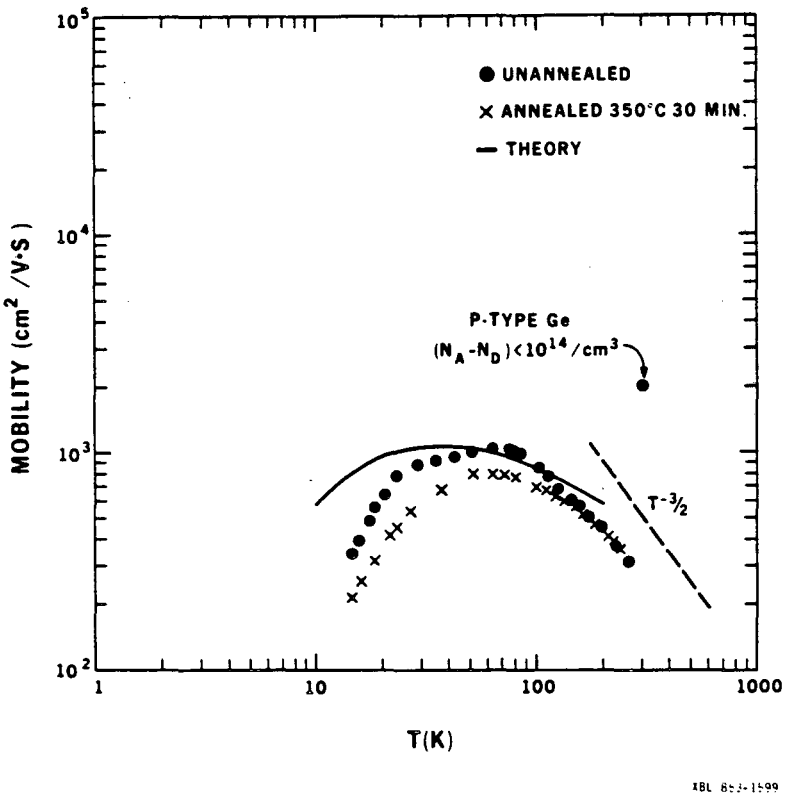

Fig. 26. Hall mobility as a function of temperature for a 100keV boron implant into Ge at a dose of 1 x $10^{14}/cm^2$.

The minor change in the mobility at T>10 K is within the fluctuation of the mobility from sample to sample and such fluctuation was also observed for lower temperature anneals. A slight increase in the mobility would be expected upon annealing of the damage related acceptor centers, as the ionized impurity concentration would decrease. However such a consistant increase is unobservable due to the fluctuations.

Figure 26 shows plots of Hall mobility versus temperature for a 100keV boron implant at a dose of $1 \times 10^{14}/cm^2$, in the "as implanted" state and after annealing at 350°C for 30 minutes. The average mobility values are lower than the lower dose sample in figure 17. This is to be expected as the ionized impurity concentration is greater, resulting in a decrease of the average mean free path.

Just as with the Hall coefficient, the Hall mobility of an implanted layer can be calculated (assuming no circulating currents) from[29]:

$$\mu_H = \frac{R_s}{\rho_s} = \frac{\int_0^t n(x)\ \mu^2(x)\ dx}{\int_0^t n(x)\ \mu(x)\ dx}$$

The lower doped regions will tend to increase the total mobility measured above that expected for the peak concentrations although the high concentration regions will still dominate. The theoretical temperature dependence of the mobility was calculated at the same time as the Hall coefficient, previously mentioned, and is also shown in figure 26. With no fitting parameters, the qualitative and quantitative agreement between experiment and theory is quite good. The

extrapolated room temperature value of the Hall mobility is the same for both the as-implanted and annealed samples, which correlates with the constant impurity concentration previously noted in figure 10.

4.4.2 Photothermal Ionization Spectroscopy

Photothermal ionization spectroscopy (PTIS) is primarily used to study shallow level impurities in semiconductors. The high energy resolution of this method makes it ideal for differentiating between different shallow levels where the ground state energies may vary by less than one meV. For our purposes, PTIS was used to determine if the relative concentration of the boron changed upon annealing in boron and BF_2 implanted samples.

PTIS involves a two step process whereby a photon of a given energy excites a bound carrier from its ground state to an excited state. If a phonon is subsequently absorbed from the lattice, the carrier can be excited into the valence band (for acceptors). The ionization of free carriers results in a photoconductive response if a bias is applied across the sample. A scan of photon energy is made and the photoconductive response is measured at a constant temperature. A series of peaks at different photon energies is subsequently generated. These peaks correspond to the excitation of holes into various bound excited states. At temperatures below 10 K practically all of the holes are bound in the ground state of shallow acceptors. At higher temperatures it is possible to get direct thermal ionization of the acceptors which leads to a rapid reduction in the signal. A good compromise temperature where sufficient phonons exist to assist the second ionization step but where direct ionization is still weak is about 7 K, for ultra-pure Ge. This method has been used to study

shallow impurities in ultra-pure germanium.[33,34,35,36] Since each shallow level has a slightly different ground state, PTIS provides an excellent means of fingerprinting each level. The major advantage of PTIS, over absorption spectroscopy, is the means by which the signal is detected. With PTIS the sample is also the detector, while in absorption spectroscopy a separate detector is required. The sensitivity for PTIS is, to a first order, impurity concentration independent. Impurity concentrations as low as 1 x $10^7/cm^3$ can be observed in 0.1 cm^3 samples. The signal strength in absorption

PHOTO THERMAL IONIZATION SPECTROSCOPY
SAMPLE GEOMETRY

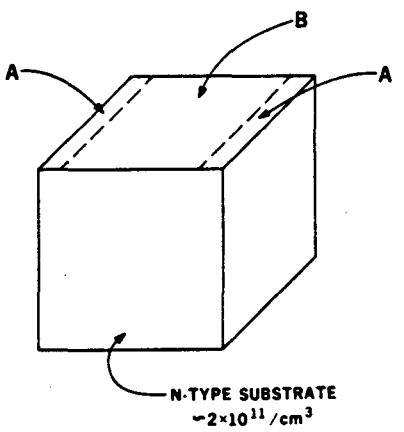

A: Ion implanted top edges and sides with center strip B masked
150keV ^{11}B $1\times10^{14}/cm^2$ annealed

B: Ion implanted top surface (mask removed) with species to be studied at 100keV $1\times10^{11}/cm^2$

Fig. 27. PTIS sample geometry for the study of implanted layers in Ge.

spectroscopy depends upon the impurity concentration. A concentration detection limit of about 5 x $10^{12}/cm^3$ can be achieved today.

The geometry of the samples for the PTIS experiments is shown in figure 27. Again, as with VTHE, an isolating n-type substrate was used insuring that any conductivity change observed during illumination

would be restricted to the p-type implanted region. Most of one surface was masked during contact implantation. After removal of the mask and annealing of the boron contacts, this surface was implanted at 100 keV with the species to be studied (either boron or BF_2) at a dose of $1 \times 10^{11}/cm^2$. Figure 28 shows a typical spectrum for an unannealed boron implant. The boron lines are apparent indicating at least some of the boron is substitutional upon implantation. The aluminum was present in the as grown crystal and its lines are useful for forming ratios with the boron lines to determine any relative concentration change upon annealing. In fact, no concentration change was observed after annealing for 30 minutes at 300°C.

The resistance of the BF_2 as-implanted layer was too high to allow any PTIS measurements ($R > 10^{10}$ ohms). However upon annealing

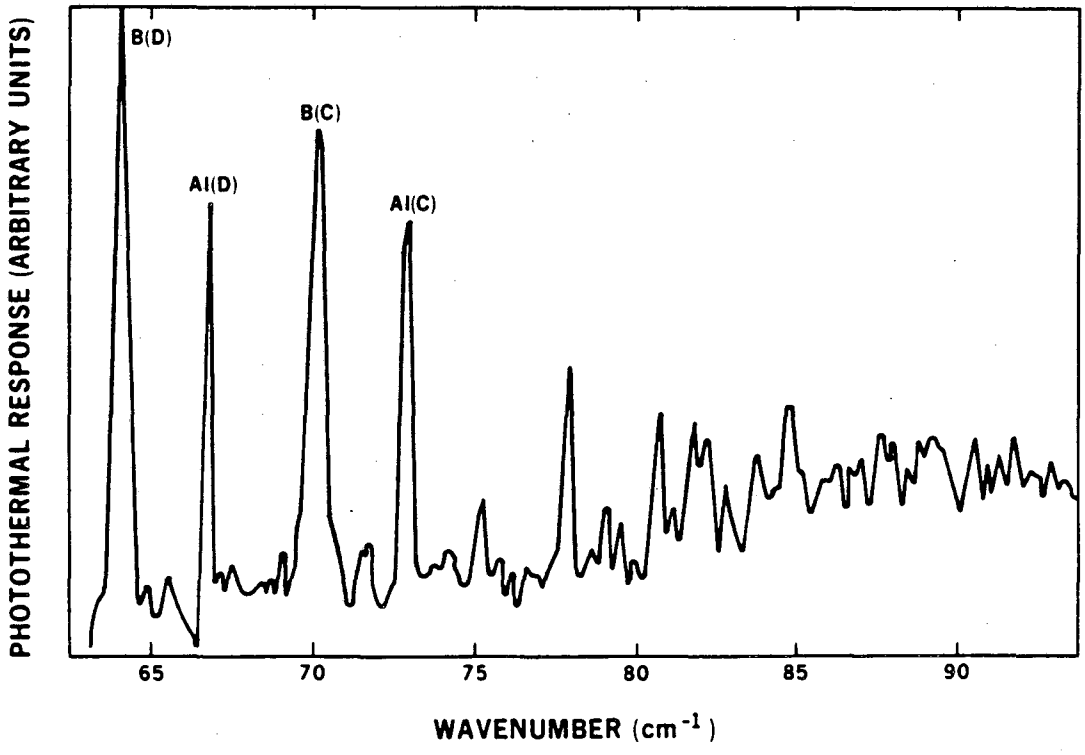

XBL 8410-4397

Fig. 28. PTIS spectrum of 100keV boron implant in Ge at a dose of $1 \times 10^{11}/cm^2$ in the unannealed condition.

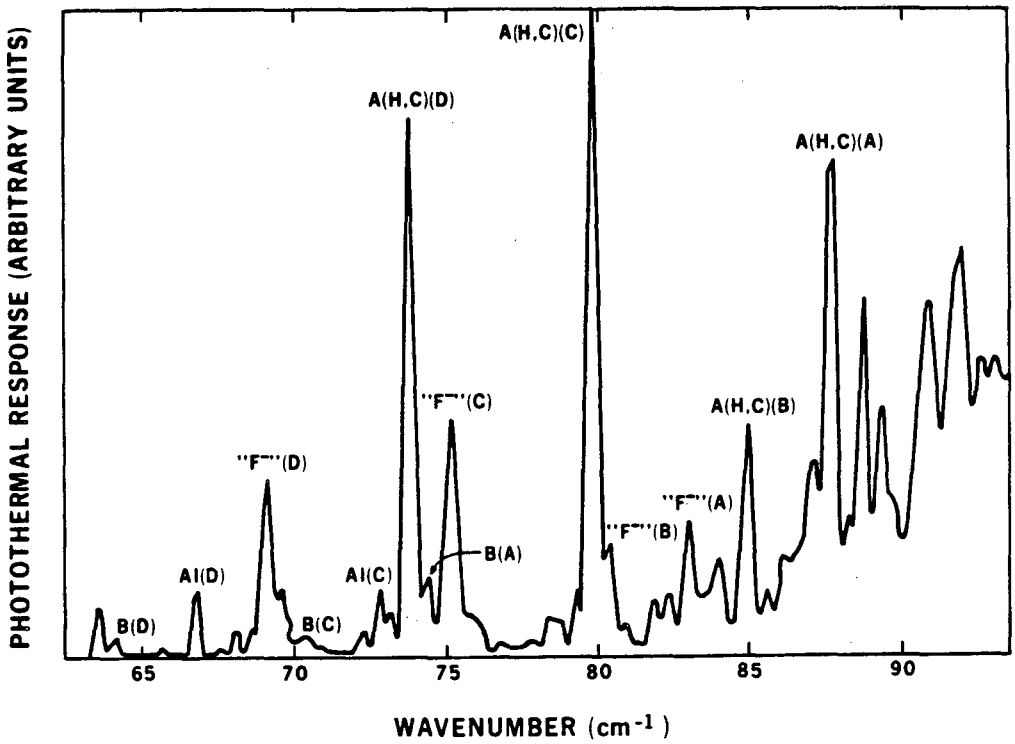

XBL 8410-4398

Fig. 30. PTIS spectrum of a 100keV BF_2 implant into Ge at a dose of $1 \times 10^{11}/cm^2$ after annealing at 300°C for 30 minutes.

at 300°C for 30 minutes the impedance dropped and the signal to noise ratio increased dramatically yielding the spectra shown in figure 29. The boron lines are again observed indicating that some of the BF_2 complexes break up either upon implantation or subsequent annealing to yield substitutional boron. In addition to the boron lines, a new series of lines which may be related to fluorine, as discussed earlier, were observed. Further investigations are required to confirm the origin of these new acceptor lines.

4.4.3 Secondary Ion Mass Spectroscopy

Secondary ion mass spectroscopy (SIMS)[37] was used to confirm the dose and distribution of the ion implanted boron. SIMS involves

the bombardment of the sample surface with a primary ion (usually $^{16}O^-$ or $^{133}Cs^+$) which in turn sputters off some of the surface atoms. Some of these sputtered atoms are ionized. These "secondary" ions are analyzed by a mass spectrometer. Oxygen enhances the positive secondary ion yield while cesium enhances the negative secondary ion yield. The lower detection limits (about $3 \times 10^{15}/cm^3$ for As in Si) are too high for high purity bulk Ge investigation, however, for implanted layers it is very useful for profiling the total implanted impurity distribution. SIMS can not yield any information on the profile of the electrically active impurities.

Samples were prepared with two implants on the same surface. Figure 29 compares the SIMS profiles with the LSS calculated profiles for 50keV and 200keV overlapping implants of boron both at a dose of 1

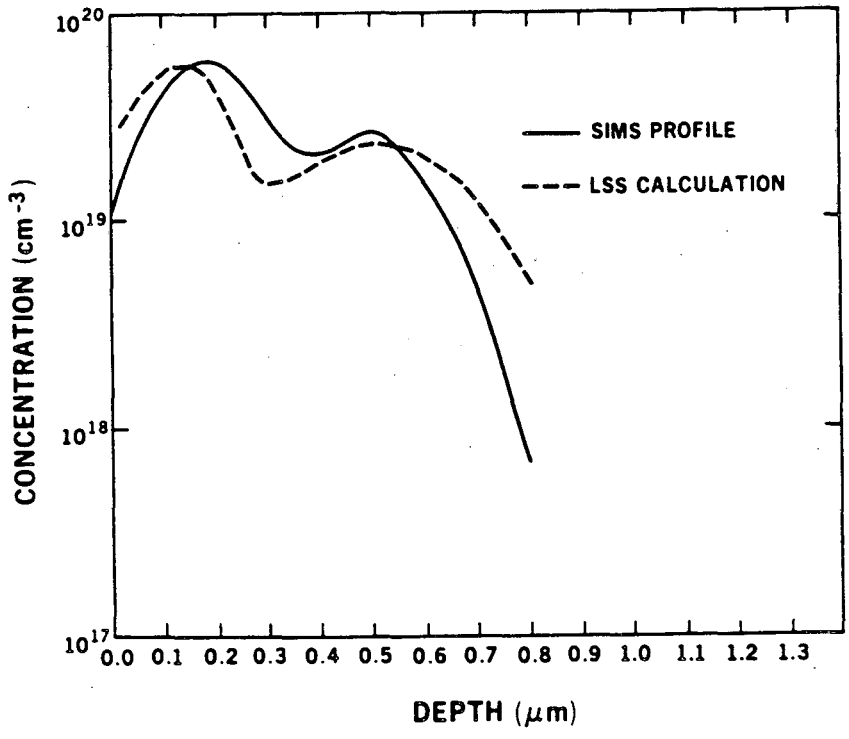

XBL 8410-4396

Fig. 29. SIMS profile of 50 and 100keV ^{11}B implants into Ge at a dose of $1 \times 10^{15}/cm^2$.

x $10^{15}/cm^2$. The comparison is reasonably good and it confirms the accuracy of the ion implantation equipments' calibration at higher doses.

5. SUMMARY AND CONCLUSIONS

$^{11}B^+$, $^{12}C^+$ and BF_2^+ ions implanted into Ge were studied using several techniques. Carrier concentration of the implanted layers as a function of implantation species, implantation dose, implantation energy and post implant annealing temperature have been investigated using Hall effect. The characterization of the damage created upon implantation using DLTS was presented. Finally Hall mobility and photothermal ionization spectroscopy results were reviewed.

The results of the experiments on boron implants indicate that over the entire dose range ($5 \times 10^{11}/cm^2$ to $1 \times 10^{14}/cm^2$) and energy range (25keV to 150keV) studied, 100% of the boron ions are substitutionally active upon implantation at room temperature. For low energy implants (25keV) of boron the concentration of stable damage related acceptor centers is significantly less than the concentration of shallow boron related acceptor centers over the entire dose range studied. As the implantation energy increases the concentration of damage related acceptor centers per incoming ion also increases. This increase in damage is more significant at lower doses than at higher doses. Thus at 100keV the concentration of damage related acceptor centers becomes greater than the concentration of shallow boron related acceptor centers at doses below $1 \times 10^{12}/cm^2$.

The damage related acceptor centers consist of three hole traps, H1, H2 and H3. None of these traps are associated with boron. Upon annealing below 225°C the concentration of H1 and H2 appears to increase. Annealing for 30 minutes at temperatures above 250°C results in the elimination of H1 and H2. Hole trap H3 is annealed

away after 30 minutes at 150°C. The hole traps H1 and H2 have been observed before by Pearton et al[26] in DLTS studies on γ-irradiated Ge. They concluded they are oxygen-vacancy related defects. H3 appears to be the same hole trap observed by Bourgoin et al[30] in electron irradiated Ge. They suggested that it may be associated with a divacancy.

The boron in BF_2 implants is not significantly electrically active upon room temperature implantation within the dose range and energy range discussed above. One possible explanation for this observation is that upon implantation at the same energy boron loses more energy through electronic stopping (phonon production) while the BF_2 loses more energy via nuclear stopping processes since it dissociates at the surface into three atoms of equal velocity. The additional heat production associated with the boron implantation may help anneal the boron into substitutional sites during implantation. The same three hole traps, H1, H2 and H3, are observed. Upon annealing at 350°C for 30 minutes the damage is repaired and the boron is substitutional. In addition to the shallow boron acceptor centers there appears to be another shallow acceptor center of comparable concentration produced upon annealing. PTIS results show a new set of acceptor lines which may correspond to fluorine behaving as an interstitial acceptor.

REFERENCES

1. Carter G and Grant W A, Ion Implantation of Semiconductors, (Halsted Press, New York, New York), 1976.
2. Alvager T and Hansen N J, Rev. Scient. Instrum. 33, 567 (1962).
3. Ponpon J P, Grob J J, Stuck R, Burger P and Siffert P, 2nd Int. Conf. on Ion Impl., (1971)
4. Herzer H and Kalbitzer S, 2nd Int. Conf. on Ion Impl., (1971)
5. Alton G D and Love L O, Can. Jour. of Phys., 46, 695 (1968).
6. Alton G D, Isotope Division, Oak Ridge Nat. Lab. Report, August (1967).
7. Sigurd D, Fladda G, Eriksson L, and Bjorkqvist K, Rad. Eff., 3, 145 (1970).
8. Muller R S and Kamins J I, Device Electronics for Integrated Circuits, (John Wiley and Sons, New York, New York), 1977.
9. Debye P P and Conwell E M, Phys. Rev., 93, 693 (1954).
10. Shockley W and Read W T, Phys. Rev., 87, 835 (1952).
11. Hall R N, Phys. Rev. 87, 387 (1952).
12. Fuller C S and Ditzenberger J A, Phys. Rev., 91, 193 (1953).
13. Lindhard J, Scharff M and Schiott H E, Mat. Fys. Medd. Dan. Vid. Selsk. 33, No. 14 (1963).
14. Gibbons J F, Johnson W S and Mylroie S W, Projected Range Statistics, (Halstead Press, Stroudsberg, Pa.), 1975.
15. Sigmund P, Appl. Phys. Lett. 14, 114 (1969).
16. Loferski J J and Rappaport P, Phys. Rev. 111, 432 (1958).
17. Vavilov V S, Smirnov L S, Galkin G N, Spitsyn A V and Patskevish V M, Sov Phys. Tech. Phys. 1, 1805 (1957).
18. Vavilov V S, Smirnov L S, Galkin G N, Spitsyn A V and Patskevish V M, Sov Phys. Tech. Phys. 3, 894 (1958).

19. Troxell J R, Solid State Electronics 26, No. 6 539 (1983).

20. Haller E E, Hueschen M R and Richards P L, Appl. Phys. Lett., 34, 495 (1979)

21. Palaio N P, Rodder M, Haller E E and Kreysa E, Lawerence Berkeley Laboratory Report 15410, Feb. 1983.

22. Mayer J W, Eriksson L, Picraux S T and Davies J A, Can. Jour. of Phys., 46, 663 (1968).

23. Johansson N G E, Mayer J W and Marsh O J, Solid State Electronics, 13, 317 (1970).

24. Tinsley A W, Jones K C, Stevens P R, George G G and Gunnersen E M, Proc. of Europ. Conf. on Ion Impl., Reading, (1970).

25. Bjorkquist K, Sigurd D, Fladda G and Bjarholt G, Rad. Eff., 6, 141 (1970).

26. Pearton S J, Tavendale A J, Kahn J M and Haller E E, Rad. Eff., 81, 293 (1984).

27. Van derPauw L J, "Phillips Res. Reports", 13, 1 (1958).

28. Fistul' V I, Heavily Doped Semiconductors, (Plenum Press, New York, New York), 1969.

29. Petritz R L, Phys. Rev., 110, 1254 (1958).

30. Borgoin J C, Mooney P M and Poulin F, Int. Conf. on Defects and Rad. Effects in Semiconductors, Oiso, Japan (1980).

31. Sze S M and Irvin J C, Solid State Electronics, 11, 599 (1968).

32. Brown D M and Bray R, Phys. Rev., 127, No. 5 (1962).

33. Skolnik M S, Eaves L, Stradling R A, Portal J C and Askenazy S, Solid State Comm., 15, 1403 (1974).

34. Haller E E and McMurray R E Jr, Physica, 116B, 349, (1983)

35. Haller E E, Hansen W L and Goulding F S, Adv. Phys., 30, 93 (1981).

36. Haller E E and Hansen W L, Sol. State Comm., 15, 687 (1974).

37. Evans C A Jr, Anal. Chem., 44 (Nov. 1972) 67A.

38. Conwell E M and Weisskopf V F, Phys. Rev., 77, 388 (1950).

39. Brooks H, Phys. Rev., 83, 879 (1951).

40. Bohm D, Quantum Mechanics, (Prentice Hall, Englewood Cliffs, New Jersey), 1951.

41. Greenberg M D, Foundations of Applied Mathematics, (Prentice Hall Inc., Englewood Cliffs, N.J.), 1978.

42. Lang D V, J. Appl. Phys., 45, 3023 (1974).

APPENDIX 1: DISCUSSION OF FREE CARRIER SCATTERING MECHANISMS IN SEMICONDUCTORS

The Bardeen-Shockley derivation of lattice mobility i.e. the effect of phonon scattering, is given by[9]

$$\mu_l = \frac{(8\pi)^{1/2} h^4 C_{11}}{3 \varepsilon_{lp}^2 (m_p^*)^{5/2} (kT)^{3/2}}$$

where ε_{lp} is the shift of the edge of the valence band per unit dilation (eV) and C_{11} is the average longitudinal elastic constant. Phonon scattering arising from acoustic phonons yield a temperature dependence for the mobility of $T^{-3/2}$. This is known to be true for p-type germanium below 70 K if the doping is less than 1×10^{14} $/cm^3$.[32] At higher temperatures the optical modes also contribute yielding a $T^{-2.3}$ temperature dependence for the mobility. At temperatures below 20 K ionized impurity scattering dominates.

The original theory describing scattering from interaction of the carrier with the screened coulomb potential of the ionized impurity was proposed by Conwell and Weisskopf[38]. In order to get convergence with their theory they "cut-off" the coulomb field of the impurity at some distance. Later Brooks and Herring[39] introduced a shielding factor into the potential to account for the screening by other electrons in the conduction band. These electrons effectively cancel the impurities' field at large distances by distributing themselves around the impurity. The Brooks-Herring formula for the relaxation time of heavy or light holes restricted to intraband scattering is

$$\frac{1}{t_{ii}^{l,h}} = \frac{N_{ii}\ \pi\ q^4}{\varepsilon_r^2 \varepsilon_o^2\ (2)^{3/2}\ (m_{l,h})^{1/2}\ E^{3/2}} [\ln(b_{l,h} + 1) - \frac{b_{l,h}}{b_{l,h} + 1}]$$

where

$$b_{l,h} = \frac{2\ \varepsilon_r \varepsilon_o\ m_{l,h}\ k\ T\ E}{\pi\ h^2\ q^2\ p'}$$

l,h indicates light or heavy holes.

$$p' = p + (\ p + N_d\ )\ (\ 1 - \frac{p + N_d}{N_a}\ )$$

$$N_{ii} = p + 2\ N_d$$

for compensated material. For relatively uncompensated material $p' = p$.

The total mean free time $t(E)$ is a combination of the effects of ionized impurity scattering $t_{ii}(E)$ and acoustic phonon scattering $t_l(E)$. They combine according to

$$\frac{1}{t(E)} = \frac{1}{t_{ii}(E)} + \frac{1}{t_l(E)}$$

The mobility using the Books-Herring formula for ionized impurity scattering is given by[9]

$$\mu_{ii} = \frac{2^{7/2}\ (\varepsilon_r \varepsilon_o)^2\ (kT)^{3/2}}{\pi^{3/2}\ (m^*)^{1/2}\ q^3\ N_I\ (\ \ln\ (\ 1 + b\ ) - \frac{b}{(1 + b)}\ )}$$

$$b = \frac{6\ \varepsilon_r \varepsilon_o\ m^*\ k^2\ T^2}{\pi\ p\ h^2\ q^2}$$

If $p = N_I$, the Brooks-Herring approximation is very close to the Conwell-Weisskopf approximation. The $T^{3/2}$ term will dominate the temperature dependence when the ionized impurity concentration becomes constant. This occurs when the free carrier concentration drops below

the compensating concentration. There is a transition region usually between 20 K and 70 K where both acoustic phonon and ionized impurity scattering are important. The mobility in this region is sucessfully predicted using the above equation for impurity concentrations below 1 x $10^{15}/cm^3$. At higher impurity concentrations the momentum difference for interband scattering becomes less thus the restriction to intraband scattering loses its validity[40]. At higher concentrations the theory tends to over estimate the mobility, i.e. by 2.2 x $10^{15}/cm^3$ the theory is already 20 percent too high[32].

APPENDIX 2: DOUBLE INTEGRATION OF A GAUSSIAN IMPURITY PROFILE

The problem is to determine the total depletion width for a given reverse bias applied to a sample with the geometry described in the experimental section on DLTS. The background doping density was 1 x $10^{10}/cm^3$ and the n-type side was a 25 keV ^{31}P implant at a dose of 1 x $10^{14}/cm^2$. Since it is the depletion into the p-type side that concerns us and the contribution of the n-type side to the total depletion width is negligible then the doping on the n-type side was assumed to equal 1 x $10^{19}/cm^3$ to help simplify the problem.

for the <u>n-type side</u>

$$\rho(x) = q\, N_d$$

$$E(x) = \int_{x_1}^{x_2} \frac{\rho(x)}{\varepsilon_r\, \varepsilon_o}\, dx = q\, N_d\, (\, x_2 - x_1\,)$$

for the <u>p-type side</u>

$$\rho(x) = -q\, \left(N_a^o + \frac{\phi}{\sigma_p \sqrt{2\,\pi}} \exp\left(- \frac{(x - x_o)^2}{2\, \sigma_p^2}\right)\right)$$

$$E(x) = - \frac{q\, N_a^o}{\varepsilon_r \varepsilon_o}\, (\, x - x_o) - \frac{q\, \phi}{\varepsilon_r \varepsilon_o\, \sigma_p \sqrt{2\pi}} \int_{x_2}^{x} \exp\left(\frac{-(\, y - x_o)^2}{2\, \sigma_p^2}\right) dy$$

Problem: Determine the total depletion width $x_3 - x_2$ (assuming $x_2 - x_1$ is negligible) for a given voltage.

Solution: Break the p-side into 2 regions. one before the peak of the implant ie $x_2 < x_3 < x_o$ and the other region after the peak ie $x_o < x_3 <$ surface.

for the p-side

$$E(x) = -\frac{q\,N_a^o}{\varepsilon_r\,\varepsilon_o}\,(\,x - x_2\,) - \frac{q\,\phi}{\varepsilon_r\varepsilon_o\,\sigma_p\sqrt{2\,\pi}}\int_{x_2}^{x}\exp\left(\frac{-(y - x_o)^2}{2\,\sigma_p^2}\right)dy$$

let $\quad x_2 = 0$

changing variables

let $\quad Z = \frac{1}{2}\,\frac{(\,y - x_o\,)}{\sigma_p}$

$$dZ = \frac{dy}{\sqrt{2}\,\sigma_p}$$

$$C = \frac{-\,q\,\phi}{\varepsilon_r\varepsilon_o\,\sigma_p\sqrt{2\,\pi}}$$

then

$$C\int_0^x \exp\left(\frac{-(\,y - x_o\,)^2}{2\,\sigma_p^2}\right)dy = C\,\sqrt{2}\,\sigma_p\int_{\frac{-x_o}{\sqrt{2}\,\sigma_p}}^{\frac{x - x_o}{\sqrt{2}\,\sigma_p}}\exp\,(\,-\,Z^2\,)\,dZ$$

by definition

$$\frac{2}{\sqrt{\pi}}\int_0^X \exp\,(\,-\,\gamma^2\,)\,d\gamma = \text{erf}\ X$$

Case 1

For $x<x_o$ (before peak)

$$C\sqrt{2}\,\sigma_p\int_{\frac{-x_o}{\sqrt{2}\,\sigma_p}}^{\frac{x-x_o}{\sqrt{2}\,\sigma_p}}\exp(-z^2)dz = C\sqrt{2}\,\sigma_p\frac{\sqrt{\pi}}{2}\left[\frac{2}{\sqrt{\pi}}\int_{\frac{-x_o}{\sqrt{2}\,\sigma_p}}^{0}\exp(-z^2)dz - \frac{2}{\sqrt{\pi}}\int_{\frac{x-x_o}{\sqrt{2}\,\sigma_p}}^{0}\exp(-z^2)dz\right]$$

$$= C\sqrt{2}\,\sigma_p\frac{\pi}{2}\left[\operatorname{erf}\left(\frac{x_o}{\sqrt{2}\,\sigma_p}\right) - \operatorname{erf}\left(\frac{x-x_o}{\sqrt{2}\,\sigma_p}\right)\right]$$

Case 2

For $x > x_o$ (after peak)

$$C\sqrt{2}\,\sigma_p\int_{\frac{-x_o}{\sqrt{2}\,\sigma_p}}^{\frac{x-x_o}{\sqrt{2}\,\sigma_p}}\exp(-z^2)dz = C\sqrt{2}\,\sigma_p\frac{\sqrt{\pi}}{2}\left[\frac{2}{\sqrt{\pi}}\int_{\frac{-x_o}{\sqrt{2}\,\sigma_p}}^{0}\exp(-z^2)dz - \frac{2}{\sqrt{\pi}}\int_{0}^{\frac{x-x_o}{\sqrt{2}\,\sigma_p}}\exp(-z^2)dz\right]$$

$$= C\sqrt{2}\,\sigma_p\frac{\sqrt{\pi}}{2}\left[\operatorname{erf}\left(\frac{x_o}{\sqrt{2}\,\sigma_p}\right) + \operatorname{erf}\left(\frac{x-x_o}{\sqrt{2}\,\sigma_p}\right)\right]$$

For Case 1

$$E(x) = -\frac{q\,N_a^o}{\epsilon_r\,\epsilon_o}(x - x_2) - \frac{q\,\phi}{2\,\epsilon_r\epsilon_o}\left[\operatorname{erf}\left(\frac{x_o}{\sqrt{2}\,\sigma_p}\right) - \operatorname{erf}\left(\frac{x-x_o}{\sqrt{2}\,\sigma_p}\right)\right]$$

$$\operatorname{erf} x \sim 1 - (a_1t + a_2t^2 + a_3t^3 + a_4t^4 + a_5t^5)\exp(-x^2)$$

where[41]

$$t = \frac{1}{1 + 0.3275911x}$$

and

a_1 through a_5 are constants i.e. $a_1 = 0.254829592$

this approximation is accurate to within $\pm 1.5 \times 10^{-7}$.

Using this approximation

$$E(x) = \frac{-q\,N_a^o}{\varepsilon_r\,\varepsilon_o}(x - x_2) - \frac{q\,\phi}{2\varepsilon_r\varepsilon_o}\Big[1 - \Big(a_1t_1 + a_2t_1^2 + a_3t_1^3 + a_4t_1^4 + a_5t_1^5\Big)\exp\Big(-\Big(\frac{x_o}{\sqrt{2}\,\sigma_p}\Big)^2\Big)\Big] + \frac{q\,\phi}{2\varepsilon_r\varepsilon_o}\Big[1 - \Big(a_1t_2 + a_2t_2^2 + a_3t_2^3 + a_4t_2^4 + a_5t_2^5\Big)\exp\Big(-\Big(\frac{x - x_o}{\sqrt{2}\,\sigma_p}\Big)^2\Big)\Big].$$

where

$$t_1 = \frac{2\,\sigma_p}{2\,\sigma_p + 0.3275911\,x_o}$$

and

$$t_2 = \frac{2\,\sigma_p}{2\,\sigma_p + 0.3275911(x - x_o)}$$

$$\phi_i + V_R = \phi_n + \phi_p = \frac{q\,N_d}{2\,\varepsilon_r\varepsilon_o}(x_2 - x_1)^2 + \frac{q\,N_a^o}{2\,\varepsilon_r\varepsilon_o}(x_3 - x_2)^2 + \frac{q\,\phi}{2\,\varepsilon_r\varepsilon_o}x_3 - \frac{a_1q\,\phi}{2\,\varepsilon_r\varepsilon_o}\int_0^{x_3} t_1\exp\Big(-\Big(\frac{x_o}{\sqrt{2}\,\sigma}\Big)^2\Big)\,dx - \frac{a_2q\,\phi}{2\,\varepsilon_r\varepsilon_o}\int_0^{x_3} t_1^2\exp\Big(-\Big(\frac{x_o}{\sqrt{2}\,\sigma}\Big)^2\Big)\,dx - \frac{a_3q\,\phi}{2\,\varepsilon_r\varepsilon_o}\int_0^{x_3} t_1^3\exp\Big(-\Big(\frac{x_o}{\sqrt{2}\,\sigma}\Big)^2\Big)\,dx - \frac{a_4q\,\phi}{2\,\varepsilon_r\varepsilon_o}\int_0^{x_3} t_1^4\exp\Big(-\Big(\frac{x_o}{\sqrt{2}\,\sigma}\Big)^2\Big)\,dx - \frac{a_5q\,\phi}{2\,\varepsilon_r\varepsilon_o}\int_0^{x_3} t_1^5\exp\Big(-\Big(\frac{x_o}{\sqrt{2}\,\sigma}\Big)^2\Big)\,dx - \frac{q\,\phi}{2\,\varepsilon_r\varepsilon_o}x_3 + \frac{q\,\phi}{2\,\varepsilon_r\varepsilon_o}\Big[a_1\int_0^{x_3} t_2\exp\Big(-\Big(\frac{x_o - x}{\sqrt{2}\,\sigma}\Big)^2\Big) + a_2\int_0^{x_3} t_2^2\exp-\Big(\frac{x_o - x}{\sqrt{2}\,\sigma}\Big)^2dx + a_3\int_0^{x_3} t_2^3\exp\Big(-\Big(\frac{x_o - x}{\sqrt{2}\,\sigma}\Big)^2\Big) + a_4\int_0^{x_3} t_2^4\exp-\Big(\frac{x_o - x}{\sqrt{2}\,\sigma}\Big)^2 +$$

$$a_5 \int_0^{x_3} t_2^5 \exp\left(- \left(\frac{x_o - x}{\sqrt{2}\sigma} \right)^2 \right) dx \;] \; .$$

$$\phi_i + V_R = \frac{q\, N_d}{2\, \epsilon_r \epsilon_o} (x_2 - x_1)^2 + \frac{q\, N_a^o}{2\, \epsilon_r \epsilon_o} (x_3 - x_2)^2 - \frac{q\, \phi}{2\, \epsilon_r \epsilon_o} \exp -\left(\frac{x_o}{\sqrt{2}\sigma}\right)^2 [$$

$$a_1 t_1 x_3 + a_2 t_1^2 x_3 + a_3 t_1^3 x_3 + a_4 t_1^4 x_3 + a_5 t_1^5 x_3] +$$

$$\frac{q\, \phi}{2\, \epsilon_r \epsilon_o} [\; a_1 \int_0^{x_3} t_2 \exp\left(- \left(\frac{x_o - x}{\sqrt{2}\sigma} \right)^2 \right) + a_2 \int_0^{x_3} t_2^2 \exp -\left(\frac{x_o - x}{\sqrt{2}\sigma}\right)^2 dx +$$

$$a_3 \int_0^{x_3} t_2^3 \exp\left(- \left(\frac{x_o - x}{\sqrt{2}\sigma} \right)^2 \right) + a_4 \int_0^{x_3} t_2^4 \exp -\left(\frac{x_o - x}{\sqrt{2}\sigma}\right)^2 dx$$

$$a_5 \int_0^{x_3} t_2^5 \exp\left(- \left(\frac{x_o - x}{\sqrt{2}\sigma} \right)^2 \right) dx \;] \; .$$

Use charge neutrality to solve for ($x_2 - x_1$)

$$q\, N_d\, (x_2\; x_1) = q \int_{x_2}^{x_3} N_a(x)\, dx$$

$$N_d\, (x_2 - x_1) = N_a^o (x_3 - x_2) + \frac{\phi}{2} \left[\operatorname{erf}\left(\frac{x_o}{\sqrt{2}\sigma}\right) - \operatorname{erf}\left(\frac{x_o - x_3}{\sqrt{2}\sigma} \right) \right]$$

$$(x_2 - x_1)^2 = \left[N_a^o (x_3 - x_2) + \frac{\phi}{2} \left[\operatorname{erf}\left(\frac{x_o}{\sqrt{2}\sigma}\right) - \operatorname{erf}\left(\frac{x_o - x_3}{\sqrt{2}\sigma} \right) \right] \frac{1}{N_d} \right]^2$$

So

$$\phi_i + V_R = \frac{q\, N_d}{2\epsilon_r \epsilon_o N_d^2} \left[N_a^o (x_3 - x_2) + \frac{\phi}{2} \left[\operatorname{erf}\left(\frac{x_o}{\sqrt{2}\sigma}\right) - \operatorname{erf}\left(\frac{x_o - x}{\sqrt{2}\sigma} \right)\right]\right]^2 +$$

$$\frac{q\,N_a^o}{2\,\varepsilon_r\varepsilon_o}\,(x_3 - x_2)^2 - \frac{q\,\phi}{2\,\varepsilon_r\varepsilon_o}\exp -\left(\frac{x_o}{\sqrt{2}\,\sigma}\right)\,[$$

$$a_1 t_1 x_3 + a_2 t_1^2 x_3 + a_3 t_1^3 x_3 + a_4 t_1^4 x_3 + a_5 t_1^5 x_3] +$$

$$\frac{q\,\phi}{2\,\varepsilon_r\varepsilon_o}\,[\,a_1\int_0^{x_3} t_2 \exp\left(-\left(\frac{x_o - x}{\sqrt{2}\,\sigma}\right)^2\right) + a_2\int_0^{x_3} t_2^2 \exp-\left(\frac{x_o - x}{\sqrt{2}\,\sigma}\right)^2 dx +$$

$$a_3\int_0^{x_3} t_2^3 \exp\left(-\left(\frac{x_o - x}{\sqrt{2}\,\sigma}\right)^2\right) + a_4\int_0^{x_3} t_2^4 \exp-\left(\frac{x_o - x}{\sqrt{2}\,\sigma}\right)^2 dx$$

$$a_5\int_0^{x_3} t_2^5 \exp\left(-\left(\frac{x_o - x}{\sqrt{2}\,\sigma}\right)^2\right) dx\,]$$

x_o is much larger than $2\,\sigma$

thus

$$\exp - \left(\frac{x_o}{\sqrt{2}\,\sigma}\right)^2 \to 0$$

and

$$\mathrm{erf}\left(\frac{x_o}{\sqrt{2}\,\sigma}\right) \to 1$$

$$\phi_i + V_R = \frac{q}{2\varepsilon_r\varepsilon_o N_d}\,[\,N_a^o\,(x_3 - x_2) - \frac{\phi}{2} + \frac{\phi}{2}\,(a_1 t_3 + a_2 t_3^2 + a_3 t_3^3 +$$

$$a_4 t_3^4 + a_5 t_3^5)\exp\left(-\left(\frac{x_o - x_3}{\sqrt{2}\,\sigma}\right)^2\right)]^2 + \frac{q\,N_a^o}{2\,\varepsilon_r\varepsilon_o}\,(x_3 - x_2)^2 +$$

$$\frac{q\,\phi}{2\,\varepsilon_r\varepsilon_o}\,[\,a_1\int_0^{x_3} t_2 \exp\left(-\left(\frac{x_o - x}{\sqrt{2}\,\sigma}\right)^2\right) + a_2\int_0^{x_3} t_2^2 \exp-\left(\frac{x_o - x}{\sqrt{2}\,\sigma}\right)^2 dx +$$

$$a_3\int_0^{x_3} t_2^3 \exp\left(-\left(\frac{x_o - x}{\sqrt{2}\,\sigma}\right)^2\right) + a_4\int_0^{x_3} t_2^4 \exp-\left(\frac{x_o - x}{\sqrt{2}\,\sigma}\right)^2 dx$$

$$a_5\int_0^{x_3} t_2^5 \exp\left(-\left(\frac{x_o - x}{\sqrt{2}\,\sigma}\right)^2\right) dx\,]$$

The integrals that are left involve the gaussian distribution. Simpsons' Rule was used to evaluate each integral. In order to increase the accuracy of the voltage drop calculation across the implant region, the point $x = 0$ was set at 2 microns deeper than the peak depth of the boron implant. The theoretical doping due to the implant is at least 5 orders of magnitude below the background N_a concentration.

<u>Case 2</u> $x > x_0$

Due to the symmetry of the gaussian distribution the additional voltage drop on the other side of the peak can be obtained by calculating the voltage drop up to the peak and then add the voltage drop associated with the difference between x and x_0.

The calculated results are shown in figure 21 along with the predicted doping distribution for the implants used in the DLTS experiments. From these calculations it can be seen that a reverse bias voltage of 8V depletes well into the implanted region.

This report was done with support from the Department of Energy. Any conclusions or opinions expressed in this report represent solely those of the author(s) and not necessarily those of The Regents of the University of California, the Lawrence Berkeley Laboratory or the Department of Energy.

Reference to a company or product name does not imply approval or recommendation of the product by the University of California or the U.S. Department of Energy to the exclusion of others that may be suitable.

TECHNICAL INFORMATION DEPARTMENT
LAWRENCE BERKELEY LABORATORY
UNIVERSITY OF CALIFORNIA
BERKELEY, CALIFORNIA 94720